A manuscript submitted to discussion forum of BG as a BG discussion paper (bg-2016-222):
Revised for comments by associate editor

Manganese and iron reduction dominate organic carbon oxidation in surface sediments of the deep Ulleung Basin, East Sea

Jung-Ho Hyun[1*], Sung-Han Kim[1], Jin-Sook Mok[1], Hyeyoun Cho[1], Tongsup Lee[2], Verona Vandieken[3] and Bo Thamdrup[4*]

[1]Department of Marine Sciences and Convergent Technology, Hanyang University, 55 Hanyangdaehak-ro, Ansan, Gyeonggi-do 15588, South Korea

[2]Department of Oceanography, Pusan National University, Busan 609-735, South Korea

[3]Institute for Chemistry and Biology of the Marine Environment, University of Oldenburg, Carl-von-Ossietzky-Str. 9-11, 26129 Oldenburg, Germany

[4]Nordic Center for Earth Evolution, Department of Biology, University of Southern Denmark, Campusvej 55, 5230 Odense M, Denmark

*Correspondence to:
Jung-Ho Hyun (hyunjh@hanyang.ac.kr)
Bo Thamdrup (bot@biology.sdu.dk)

Abstract. Rates and pathways of benthic organic carbon (C_{org}) oxidation were investigated in surface sediments of the Ulleung Basin (UB) characterized by high organic carbon contents (> 2.5 %, dry wt.) and very high contents of Mn oxides (> 200 μmol cm^{-3}) and Fe oxides (up to 100 μmol cm^{-3}). The combination of geochemical analyses and independently executed metabolic rate measurements revealed that Mn and Fe reduction were the dominant C_{org} oxidation pathways in the center of the UB, comprising 45 % and 20 % of total C_{org} oxidation, respectively. By contrast, sulfate reduction was the dominant C_{org} oxidation pathway accounting for 50 % of total C_{org} mineralization in sediments of the continental slope. The relative significance of each C_{org} oxidation pathway matched the depth distribution of the respective electron acceptors. The relative importance of Mn reduction for C_{org} oxidation displays saturation kinetics with respect to Mn oxide content with a low half-saturation value of 8.6 μmol cm^{-3}, which further implies that Mn reduction can be a dominant C_{org} oxidation process even in sediments with lower MnO_2 content as known from several other locations. This is the first report of a high contribution of manganese reduction to C_{org} oxidation in offshore sediments on the Asian margin. The high manganese oxide content in the surface sediment in the central UB was maintained by an extreme degree of recycling, with each Mn atom on average being reoxidized ~3800 times before permanent burial. This is the highest degree of recycling so far reported for Mn-rich sediments, and it appears linked to the high benthic mineralization rates resulting from the high organic carbon content that indicate the UB as a biogeochemical hotspot for turnover of organic matter and nutrient regeneration.

Keywords. Benthic mineralization, Manganese reduction, Iron reduction, Sulfate reduction, Ulleung Basin, East Sea

1 Introduction

Although they cover only 15 % (47×10^6 km^2) of the ocean surface area, sediments of continental margins (200–2000 m depth) are characterized by enhanced organic matter flux generated either by vertical transport from the highly productive overlying water column or by lateral transport from adjacent shelves, and thus play an important role in deposition and mineralization of organic matter (Romankevich, 1984; Jahnke et al., 1990; Walsh, 1991; Jahnke and Jahnke, 2000). Organic particles that reach the seafloor are quickly mineralized by hydrolysis, fermentation, and a variety of respiratory processes using different electron acceptors such as oxygen, nitrate, Mn oxides, Fe oxides, and sulfate (Froelich et al., 1979; Jørgensen, 2006). The partitioning of organic carbon (C_{org}) oxidation among the different electron accepting pathways has profound influence on the distribution and the release and/or retention of Mn, Fe, S and nutrients (nitrogen and phosphate) (Canfield et al., 2005; Hansen et al., 2006; Jørgensen, 2006; Slomp et al., 2013). Therefore, it is particularly important to elucidate the contribution of each C_{org} oxidation pathway in order to better understand the role of sediments in biogeochemical element cycles.

The relative significance of each carbon oxidation pathway is largely controlled by the combination of organic matter supply and availability of electron acceptors. In general, aerobic metabolism dominates the organic matter mineralization in deep-sea sediments that are characterized by low organic matter content (Jahnke et al., 1982; Glud, 2008), especially in organic carbon-starved deep-sea sediments with low sedimentation rates (Mewes et al., 2014, 2016; D'Hondt et al. 2015; Mogollón et al., 2016). In contrast, owing to high sulfate concentrations in marine sediment, sulfate reduction might account for up to 50 % of total carbon oxidation in continental margins with high organic matter flux (Jørgensen, 1982; Jørgensen and Kasten, 2006; Bowles et al., 2014). However, in sediments where manganese and iron oxides are abundant or rapidly recycled, microbial reduction of manganese and iron can be the dominant electron accepting processes over sulfate reduction (Sørensen and Jørgensen, 1987; Aller, 1990; Canfield et al., 1993b). The significance of dissimilatory iron reduction for C_{org} oxidation is well established in the sediments of various continental margins and coastal wetlands (Thamdrup, 2000; Thamdrup and Canfield, 1996; Jensen et al., 2003, Kostka et al., 2002a, 2002b; Vandieken et al., 2006; Hyun et al., 2007, 2009b). However, only a few locations such as the Panama Basin (Aller, 1990), the coastal Norwegian trough in Skagerrak and an adjacent fjord (Canfield et al., 1993a, 1993b;

Vandieken et al., 2014), the Black Sea shelf (Thamdrup et al., 2000) and the continental shelf of the northern Barents Sea (Vandieken et al., 2006; Nickel et al., 2008) are known where microbial manganese reduction significantly contributes to carbon mineralization.

The East Sea (often referred to as Japan Sea), located in the far eastern part of the Eurasian continental margin, consists of three major basins deeper than 2000 m, the Japan Basin, the Yamato Basin and the Ulleung Basin (Fig. 1). Compared to the other two basins, the surface waters of the Ulleung Basin (UB) are characterized by higher phytoplankton biomass and primary production (Yamada et al., 2005; Yoo and Park, 2009), which is associated with coastal upwelling (Hyun et al., 2009a). The enhanced biological production in the euphotic zone of the UB is responsible for the high organic carbon content (> 2.5 % wt) in the sediment, and the highest rates of C_{org} oxidation compared to other deep-sea sediments with similar depth range (Lee et al., 2008; Hyun et al., 2010). An intriguing geochemical property of the UB surface sediment is the high content of Mn oxides (> 200 μmol cm^{-3}) and Fe oxides (up to 100 μmol cm^{-3}) (Cha et al., 2007; Hyun et al., 2010). In accordance with these geochemical findings, the suppression of sulfate reduction (Hyun et al., 2010) and accumulation of Mn^{2+} in anoxic incubation of surface sediment (Vandieken et al., 2012) strongly implied that the C_{org} oxidation in the surface sediment of the UB is dominated by microbial manganese and iron reduction, but actual rates and partitioning of each electron accepting pathway in C_{org} oxidation remain to be determined in this deep marginal sediment underlying highly productive surface waters.

The primary objective of this paper was to characterize the sediment biogeochemistry with regard to the rate of C_{org} oxidation and partitioning of major terminal electron accepting pathways at two contrasting sites at the continental slope and rise in the UB. Here, for the first time in sediments of the Asian marginal seas, we document that Mn and Fe reduction are the dominant C_{org} oxidation pathways accounting for respectively 45 % and 20 % of total C_{org} oxidation in the center of the UB, and suggest that Mn and Fe reduction may be of greater importance in deep-sea sediments than previously recognized.

2 Materials and methods

2.1 Study site

The East Sea is a marginal sea surrounded by the east Asian continent and Japanese Islands

(Fig. 1, Kang et al., 2010; Liu et al., 2010). The UB located in the southwestern part of the East Sea is a bowl-shaped deep basin (2000–3000 m depth) (Fig. 1) delimited by continental slopes of Korean Peninsula and the southwestern Japanese Archipelago on the west and south, respectively, and by the Korea Plateau and the Oki Bank on the north and east, respectively (Chough et al., 2000).

Shipboard experiments were conducted in June, 2009 at two sites on the continental slope (Station M1, hereafter M1) and in the center (Station D3, hereafter D3) of the UB (Fig. 1, Table 1). Surface sediments consist of fine-grained clay with a mean grain size less than 0.004 mm in diameter (Cha et al., 2007). Two stations were characterized by two contrasting sediment colors. The Mn oxide-enriched surface sediment at the basin site (D3) was reddish-brown, whereas at the slope site (M1) it exhibited the typical gray-brown color of muddy continental margin sediments (Fig. 1). Further environmental properties are listed in Table 1.

2.2 Sampling and handling

Sediment samples were collected with a box corer. Onboard, duplicate or mostly triplicate sub-samples for geochemical analyses were collected using acrylic cores (6–9 cm in diameter and 30–40 cm in length). The sub-cores for geochemical analyses were immediately sealed with butyl rubber stoppers and transferred to a N_2-filled glove bag for sectioning and loading into polypropylene centrifuge tubes that were then tightly capped and centrifuged for 15 min at 5000 × *g*. After reintroduction into the N_2-filled glove bag, pore-waters were sampled and filtered through 0.2-μm cellulose ester syringe filters (ADVANTEC, Toyo Rashi Kaisha, Ltd). One to two mL of pore water to determine NH_4^+ was fixed with saturated $HgCl_2$, and frozen. For determination of Fe^{2+}, Mn, SO_4^{2-} and Ca^{2+}, 2 mL of the pore water were acidified with 12 M HCl and stored at 4 ℃. Pore-water for sulfide analysis was preserved with Zn acetate (20 %). Sediments for solid-phase analysis were frozen at −25 ℃ for future analyses.

2.3 Anoxic bag incubations

Anaerobic carbon mineralization rates and dissimilatory Mn and Fe reduction rates were determined in batch incubations based on the procedures of Canfield et al. (1993b) and Thamdrup and Canfield (1996). Sediment cores were transferred to a N_2-filled glove bag and sliced in 2-cm intervals to a depth of 10 cm. Sediment from parallel sections was pooled,

mixed and loaded into gas-tight plastic bags (Hansen et al., 2000). The bags were sealed without gas space, and incubated in the dark at near in situ temperature (ca. 1–2 °C) in larger N_2 filled bags to ensure anoxic conditions. Over a period of 18 days of incubation, sub-samples to determine the accumulation of total dissolved inorganic carbon (DIC) and Mn in pore water were withdrawn on days 0, 1, 3, 5, 9 and 18. Two 50-mL centrifuge tubes per bag were filled completely with sediment in a N_2-filled glove bag, and pore-water was extracted as described above. For DIC analysis, we collected 1.8 mL aliquots into glass vials without head space, fixed with 18 µL of $HgCl_2$ (125 mM), and stored at 4 °C until analysis within 4 weeks. Samples for Mn analysis were acidified with 12 M HCl and stored at 4 °C. Sediment remaining after the collection of pore water was frozen at −25 °C for later analysis of oxalate extractable solid Fe(II).

2.4 Pore-water analyses

Total dissolved inorganic carbon (DIC) and NH_4^+ were measured by flow injection analysis with conductivity detection (Hall and Aller, 1992). Nitrate was measured spectrophotometrically (Parsons et al., 1984). Dissolved Fe^{2+} was determined by colorimetric method with Ferrozine (Stookey, 1970). Dissolved Mn^{2+} and Ca^{2+} were analyzed in acidified pore water by inductively coupled plasma-atomic emission spectrometry (ICP-AES, Optima 3300DV, Perkin-Elmer Co.) and flame atomic absorption spectrometer (SpectrAA 220/FS, Varian), respectively (Thamdrup and Canfield, 1996). Dissolved sulfide was determined by the methylene blue method (Cline, 1969). Sulfate concentrations were measured using ion chromatography (Metrohm 761). The detection limit of H_2S, Ca^{2+}, Mn^{2+} and Fe^{2+} was 3 µM, 1.8 µM, 3 µM and 1 µM, respectively. Reproducibility of DIC and NH_4^+ was better than 10 %. Precision of NO_3^- was 1–2 %.

2.5 Solid-phase analyses

Total oxalate-extractable Fe [Fe(II) + Fe(III)] was extracted from air-dried sediment in a 0.2 M oxic oxalate solution (pH 3) for 4 h (Thamdrup and Canfield, 1996), and Fe(II) was extracted from frozen sediment in anoxic oxalate (Phillips and Lovley, 1987). The total oxalate-extractable Fe and Fe(II), hereafter total $Fe_{(oxal)}$ and $Fe(II)_{(oxal)}$, were determined as described for the pore-water analysis of Fe^{2+}. Oxalate-extractable Fe(III), hereafter

188 $Fe(III)_{(oxal)}$, was defined as the difference between total $Fe_{(oxal)}$ and $Fe(II)_{(oxal)}$. This fraction
189 represents poorly crystalline Fe(III) oxides. Particulate Mn, hereafter $Mn_{(DCA)}$ was extracted
190 with dithionite-citrate-acetic acid (DCA; pH 4.8) for 4 h from air-dried sediment and was
191 determined by inductively coupled plasma-atomic emission spectrometry (ICP-AES, Optima
192 3300DV, Perkin-Elmer Co). The DCA extraction aims at dissolving free Mn oxides and
193 authigenic Mn(II) phases. The reproducibility of the measurements was better than 10 % and
194 the detection limits was 3 μM for Mn and 1 μM for Fe. For the determination of total reduced
195 sulfur (TRS) that includes acid volatile sulfide (AVS = FeS + H_2S and small amounts of other
196 metal sulfides, see Rickard and Morse, 2005; Luther, 2005) and chromium-reducible sulfur
197 (CRS = S^0 + FeS_2), sediment samples were fixed with Zn acetate, and sulfide was determined
198 according to the method of Cline (1969) after a two-step distillation with cold 12 M HCl and
199 boiling 0.5 M Cr^{2+} solution (Fossing and Jørgensen, 1989). The contents of particulate
200 organic carbon (POC) and nitrogen (PON) in the surface sediment were analyzed using a
201 CHN analyzer (CE Instrument, EA 1110) after removing $CaCO_3$ using 12 M HCl.
202
203 **2.6 Oxygen micro-profiles**
204
205 Oxygen profiles were measured at 50 μm resolution using Clark-type microelectrodes
206 (Unisense, OX-50) while stirring the overlying water. Microelectrodes were calibrated
207 between 100 % air-saturated *in situ* bottom water and N_2 purged anoxic bottom water. Three
208 profiles were measured at each site. The diffusive boundary layer (DBL) and sediment-water
209 interface (SWI) were determined according to Jørgensen and Revsbech (1985). To estimate
210 the volume-specific oxygen consumption rate, we used the PROFILE software (Berg et al.,
211 1998).
212
213 **2.7 Rate measurements**
214
215 The diffusive oxygen uptake (DOU) was calculated from the calibrated oxygen microprofiles.
216
217 $$DOU = -D_o \times (\Delta C/\Delta z) \quad (1)$$
218
219 where D_o (1.07×10^{-9} m^2 s^{-1} at M1 and 1.03×10^{-9} m^2 s^{-1} at D3) is the temperature-corrected
220 molecular diffusion coefficient estimated from Schulz (2006), and C is the oxygen

concentration at depth z within the diffusive boundary layer (DBL) (Jørgensen and Revsbech, 1985).

The volume-specific O_2 consumption rates exhibited a bimodal depth distribution (see results section 3.2) with activity peaks near the sediment-water interface and the oxic/anoxic interface, respectively. Thus, O_2 consumption rates by aerobic organotrophic respiration was defined as the O_2 consumption rate near the sediment-water interface, whereas the oxygen consumption at the oxic-anoxic interface was assigned to re-oxidation of reduced inorganic compounds (Rasmussen and Jørgensen, 1992; Canfield et al., 2005).

Total anaerobic C_{org} mineralization rates were determined by linear regression of the accumulation of total DIC with time during the anoxic bag incubations (Fig. 3) after correcting for $CaCO_3$ precipitation (Thamdrup et al., 2000). Briefly, $CaCO_3$ precipitation was calculated from decreasing dissolved Ca^{2+} concentration during the anoxic bag incubation:

$$\Delta CaCO_3 = \Delta[Ca^{2+}]_{sol} \times (1+K_{Ca}) \quad (2)$$

where, K_{Ca} is the adsorption constant for Ca^{2+} (K_{Ca} = 1.6) (Li and Gregory, 1974). Then the DIC production rate corrected for $CaCO_3$ precipitation was calculated as:

$$\text{DIC production} = \text{DIC accumulation} + CaCO_3 \text{ precipitation} \quad (3)$$

Fe(III) reduction rates were determined by linear regression of the increase in solid-phase $Fe(II)_{(oxal)}$ content with time during anoxic bag incubations. The dissimilatory microbial Fe(III) reduction rate was derived by subtracting abiotic Fe reduction coupled to the oxidation of sulfide produced by sulfate reduction (Gribsholt et al., 2003):

$$\text{Dissimilatory microbial Fe(III) Red} = \text{Total Fe(III) Red} - \text{Abiotic Fe(III) Red} \quad (4)$$

assuming that abiotic Fe reduction coupled to H_2S oxidation occurred at a stoichiometry of 2 Fe(III) per 3 H_2S (Pyzik and Sommer, 1981; Melton et al., 2014):

$$2FeOOH + 3H_2S_{(\text{produced by SR})} = 2FeS + S^o + 4H_2O \quad (5)$$

Finally, to estimate the C_{org} oxidation by microbial Fe reduction, the 4:1 stoichiometry of

iron reduction coupled to C_{org} oxidation was used from the stoichiometric equation (Canfield et al., 1993a):

$$CH_2O + 4FeOOH + 8H^+ = CO_2 + 4Fe^{2+} + 7H_2O \quad (6)$$

Mn reduction rates were determined from linear regression of the production of dissolved Mn^{2+} with time during the anoxic bag incubations. Similar to previous studies (e.g., Canfield et al., 1993a, 1993b; Thamdrup and Dalsgaard, 2000), we assumed that accumulating dissolved Mn was Mn^{2+}. This ignores a potential contribution from Mn^{3+}, which in some cases can constitute a substantial fraction of the dissolved Mn pool at the upper boundary of the zone with soluble Mn accumulation in marine sediments (Madison et al., 2013). Further studies of the dynamics of soluble Mn^{3+} are required to evaluate its potential importance in anoxic incubations. Such studies pending, we find justification for our assumption in the good agreement observed in the previous studies between Mn reduction rates calculated based on the assumption that soluble Mn is Mn^{2+} (Eq. 7) and independent estimates of rates of carbon mineralization through dissimilatory Mn reduction based on DIC or NH_4^+ accumulation. Due to strong adsorption of Mn^{2+} to Mn oxide surfaces (Canfield et al., 1993b), the Mn reduction rates were estimated after compensating for the adsorption effect of Mn^{2+} to Mn-oxides according to Thamdrup and Dalsgaard (2000):

$$\text{Mn reduction rate} = Mn^{2+} \text{ accumulation rate} \times (1 + K^*_{Mn}{}^{2+} \times (1 - \Phi) \times \Phi^{-1} \times \delta_s) \quad (7)$$

where, Φ = porosity

δ_s = density of sediment

$K^*_{Mn}{}^{2+} = 4.8 + 0.14 \times [Mn(IV)]$ (ml g^{-1})

[Mn(IV)] = the content of Mn(IV) (μmol g^{-1})

We here assume that extracted $Mn_{(DCA)}$ represents Mn(IV) as observed in surface sediments of another Mn-rich site (Canfield et al., 1993b; Thamdrup and Dalsgaard, 2000). Small levels of $Mn_{(DCA)}$ remaining at depth further suggest that little Mn(II) accumulates in the solid phase (*see* Results). C_{org} oxidation by dissimilatory Mn(IV) reduction was calculated from the stoichiometric equation (Canfield et al., 1993a):

$$CH_2O + 2MnO_2 + 4H^+ = CO_2 + 2Mn^{2+} + 3H_2O \quad (8)$$

Sulfate reduction rates were determined using the radiotracer method of Jørgensen (1978). Sediment cores (35 cm long with 2.9 cm i.d.) were collected in triplicate, injected horizontally at 1-cm vertical interval with 5 µL radiolabeled sulfate ($^{35}S\text{-}SO_4^{2-}$, 15 kBq μl^{-1}, Amersham) diluted in sterilized NaCl solution (3.0 %), and incubated for 12 h at *in situ* temperature. At the end of the incubation, the sediment was sliced into sections, fixed in Zn acetate (20 %), and frozen at −25 °C until processed in the laboratory. The reduced ^{35}S was recovered using distillation with a boiling acidic Cr^{2+} solution according to Fossing and Jørgensen (1989). Background radioactivity of ^{35}S was 32.4 ± 3.7 cpm cm^{-3} (n = 10) at site D3 and 87.5 ± 38.7 cpm cm^{-3} (n = 10) at site M1. Detection limits of the SRR, estimated from the double standard deviation of the blank value (i.e., 7.4 and 77.4 cpm) according to Fossing et al. (2000), ranged from 0.79 to 2.62 nmol cm^{-3} d^{-1}. To elucidate the contribution of sulfate reduction in anaerobic carbon oxidation, the SRRs (Fig. 5B, 5G) were converted to carbon oxidation using a stoichiometric equation (Thamdrup and Canfield, 1996):

$$2CH_2O + SO_4^{2-} + 2H^+ = 2CO_2 + H_2S + 2H_2O \quad (9)$$

3 Results

3.1 Pore-water and solid-phase constituents

The depth distributions of NH_4^+, NO_3^-, Mn^{2+} and Fe^{2+} in the pore-water as well as solid phase Mn, Fe and S for the two stations are shown in Fig. 2. NH_4^+ concentrations at M1 increased steadily with depth (Fig. 2A) whereas at D3 it decreased down to 3 cm depth before it increased below (Fig. 2F). Highest concentrations of nitrate were measured at 0 to 1 cm sediment depth at the two stations and concentrations decreased below a background level (< 2 µM) below 1 cm at both M1 and D3 (Fig. 2A, 2F). Dissolved Mn^{2+} concentrations differed widely between the sites showing a maximum of 56 µM between 0 and 3 cm depth and not exceeding 10 µM below at M1 (Fig. 2B), whereas at D3 concentrations increased to a maximum of 286 µM at 10–12 cm depth (Fig. 2G). Conversely, dissolved Fe^{2+} concentrations

at M1 increased from 11 µM at 0–0.5 cm to 32 µM at 6–7 cm depth, and stayed constant below (Fig. 2C), whereas at D3, concentrations were uniformly low showing a slight increase to 12 µM at 15 cm (Fig. 2H).

Extractable Mn ($Mn_{(DCA)}$) contents were low (< 3 µmol cm^{-3}) in the upper 20 cm at the slope site (M1) (Fig. 2B), but up to 200 µmol cm^{-3} in the upper 4 cm depth of the sediment at the center of the basin (D3), with a sharp decrease to near depletion (~1 µmol cm^{-3}) below 10 cm (Fig. 2G). At the slope site (M1), contents of $Fe(III)_{(oxal)}$ decreased slightly with increasing depth from 28 µmol cm^{-3} near the surface to 13 µmol cm^{-3} at 20 cm depth, mirroring an increase in $Fe(II)_{(oxal)}$ (Fig. 2D). At the center of the basin (D3), $Fe(III)_{(oxal)}$ increased slightly from 67 µmol cm^{-3} at 0–0.5 cm to 90 µmol cm^{-3} at 4–6 cm depth, and decreased steeply below to 4.8 µmol cm^{-3} at 12–14 cm depth (Fig. 2I). Of total $Fe_{(oxal)}$, $Fe(III)_{(oxal)}$ comprised > 98 % at 0–2 cm and > 97 % at 0–8 cm depth at M1 and D3, respectively. The fraction of $Fe(III)_{(oxal)}$ in $Fe_{(oxal)}$ then decreased to 40 % at 10–12 cm depth at both sites. Acid volatile sulfur (AVS) exhibited a slight increase with depth at M1 from 0.8 µmol cm^{-3} at the surface to 7.2 µmol cm^{-3} at 20 cm depth (Fig. 2E), but was not detected at D3 (Fig. 2J). Chromium reducible sulfur (CRS) contents at M1 increased rapidly with depth from 1.9 µmol cm^{-3} at 0–0.5 cm to 21.8 µmol cm^{-3} at 20 cm depth (Fig. 2E), whereas the CRS contents remained < 0.1 µmol cm^{-3} at D3 (Fig. 2J).

3.2 O_2 microprofiles and diffusive oxygen uptake rate

Oxygen penetrated less than 4 mm into the sediments (Fig. 3), and rates of diffusive oxygen uptake (DOU) were 7.1 and 6.0 mmol O_2 m^{-2} d^{-1} at M1 and D3, respectively (Table 2). Oxygen consumption by aerobic respiration estimated from the O_2 micro-profiles (area I and II in Fig. 3) was higher at the M1 in the slope site (4.0 mmol O_2 m^{-2} d^{-1}) than at the D3 in the center of the basin (2.5 mmol O_2 m^{-2} d^{-1}). O_2 consumption by re-oxidation of reduced inorganic compounds indicated by increased activity at the oxic/anoxic interface (area III in Fig. 3) accounted for 43 % and 57 % of the DOU at M1 and D3, respectively. From the profiles of geochemical constituents (Fig. 2), O_2 consumption was mainly attributed to the re-oxidation of sulfide and Fe^{2+} at M1 and of Mn^{2+} at D3.

3.3 Anoxic bag incubations

Changes in concentrations of DIC, Ca^{2+} and dissolved Mn^{2+} and solid $Fe(II)_{(oxal)}$ contents over time during anoxic bag incubations from sediment of 0–2, 2–4, 4–6 and 6–8 cm depth intervals are presented in Fig. 4. The DIC concentrations increased linearly over time during incubations of sediment in all bags from M1 and D3, except the bag from 6–8 cm at D3. The DIC accumulation rates were generally higher at the slope site (M1) than at the basin site (D3) (Table 4). The concentrations of Ca^{2+} decreased with time at all depth intervals of M1, whereas a decrease of Ca^{2+} was observed only for the 2–4 cm depth interval at D3. The decrease of Ca^{2+} indicates $CaCO_3$ precipitation, which consequently underestimates DIC accumulation, especially at M1.

Coinciding with high solid $Mn_{(DCA)}$ contents (Fig. 2G), prominent Mn^{2+} accumulation appeared at 0–6 cm depth of D3, whereas no increase of Mn^{2+} was observed at M1 except a slight accumulation at 0–2 cm interval (Fig. 4). Solid $Fe(II)_{(oxal)}$ contents increased linearly with time at 0–4 cm depth of M1, whereas highest $Fe(II)_{(oxal)}$ accumulation was observed at 4–6 cm depth at D3. An increase of $Fe(II)_{(oxal)}$ was not discernible in the Mn-oxide-rich surface sediment (0–2 cm) of D3.

3.4 Sulfate reduction rates (SRR)

At the slope site (M1), SRR increased from 18 nmol cm^{-3} d^{-1} at the surface to 97–103 nmol cm^{-3} d^{-1} at 1.5–2 cm depth, and decreased below to 12.5 nmol cm^{-3} d^{-1} at 20 cm depth (Fig. 5B). In contrast, SRR at the manganese oxide-rich basin site (D3) ranged from 1.7 to 8.7 nmol cm^{-3} d^{-1}, and did not vary with depth (Fig. 5G). Depth integrated SRR down to 10 cm depth was 10 times higher at M1 (4.3 mmol m^{-2} d^{-1}) than at D3 (0.4 mmol m^{-2} d^{-1}) (Table 3).

3.5 DIC production rates

Vertical profiles of the DIC production rate that were derived from the linear regression of the DIC production measured in anoxic bag incubation (Fig. 4) after correcting for $CaCO_3$ precipitation, are presented in Fig. 5C and 5H for M1 and D3, respectively. At M1, the DIC production rates decreased with depth from 280 nmol cm^{-3} d^{-1} (0–2 cm depth) to 69 nmol cm^{-3} d^{-1} (8–10 cm depth) (Fig. 5C), whereas the DIC production rates at D3 were relatively similar across the upper 6 cm ranging from 86 to 136 nmol cm^{-3} d^{-1}, and decreased to 8–15 nmol cm^{-3} d^{-1} at 6–10 cm (Fig. 5H). The integrated DIC production rate within 10 cm depth

of the sediment was twice as high at M1 (14.0 mmol m^{-2} d^{-1}) as at the D3 (7.2 mmol m^{-2} d^{-1}) (Table 4).

3.6 Rates of Mn and Fe reduction

The accumulation of Mn^{2+} presented evidence that manganese reduction was occurring in the surface sediment (0–6 cm) of D3 (Fig. 4). The manganese reduction rate (MnRR) derived from Mn^{2+} accumulation with correction for adsorption ranged from 7.5 nmol cm^{-3} d^{-1} (0–2 cm depth) to 198 nmol cm^{-3} d^{-1} (2–4 cm depth) at D3 (Fig. 5I). In contrast, MnRR at M1 was indiscernible except for low activity (2.2 nmol cm^{-3} d^{-1}) at 0–2 cm depth (Fig. 5D). Depth integrated MnRR at D3 (8.21 mmol m^{-2} d^{-1}) was 200 times higher than the MnRR at M1 (0.04 mmol m^{-2} d^{-1}) (Table 3). The iron reduction rate (FeRR), derived from $Fe(II)_{(oxal)}$ accumulation, at M1 was highest in the 0–2 cm interval (237 nmol cm^{-3} d^{-1}), and then decreased with depth to 38 nmol cm^{-3} d^{-1} at 8–10 cm depth (Fig. 5E). In contrast, Fe reduction was not detected in the surface sediment at D3, but increased to its maximum rate of 240 nmol cm^{-3} d^{-1} at 4–6 cm depth. The FeRR then decreased with depth to 12 nmol cm^{-3} d^{-1} at 8–10 cm (Fig. 5J) where a few data points were adopted to derive the line of best-fit regression. Depth integrated total FeRR was slightly higher at M1 (11.4 mmol m^{-2} d^{-1}) than at D3 (7.53 mmol m^{-2} d^{-1}) (Table 3). The ratio of microbial Fe reduction, $Fe\ Red_{(microbial)}$, to abiotic Fe reduction coupled to sulfide oxidation, $Fe\ Red_{(abiotic)}$, ranged from 1.14 (8–10 cm at M1) to 52.3 (2–4 cm at D3), which indicated that the Fe reduction at Mn- and Fe oxides rich basin site was mostly a microbiologically mediated process (Table 3).

4 Discussion

4.1 Partitioning of C_{org} oxidation in accordance with the distribution of terminal electron acceptors

One of the most prominent features revealed from the vertical distributions of geochemical constituents at the basin site (D3) was that electron acceptors such as O_2, nitrate, Mn- and Fe oxides were systematically distributed with discrete zonation according to the order of decreasing energy yield for C_{org} oxidation (Fig. 5F). Such biogeochemical zones are not sharply separated in most aquatic sediments due to, e.g., sediment heterogeneity and mixing

resulting from bioirrigation, bioturbation, and bottom turbidity currents. The profiles of dissolved and solid phase geochemical constituents in the sediment provide indications as to specific diagenetic reactions prevailing (Froelich et al., 1979). However, reoxidation of reduced inorganic compounds often mask the primary reactions involved in carbon oxidation (Sørensen and Jørgensen, 1987; Hines et al., 1991). Together with the discrete geochemical zonation of the electron acceptors, the independently executed metabolic rate measurements (Fig. 5) allowed us to evaluate the relative contribution of each terminal electron-accepting pathway with sediment depth.

Previous experimental studies that have quantified pathways of anaerobic carbon oxidation in subtidal marine sediments have generally determined the contributions of Mn and Fe reduction indirectly from the difference between rates of DIC production and sulfate reduction converted to carbon equivalents (e.g., Canfield et al., 1993b; Thamdrup and Canfield, 1996; Vandieken et al., 2006). The inferred rates of Mn and Fe reduction were further supported by the depth distribution of metal oxides and patterns of Mn^{2+} and Fe^{2+} accumulation in the pore water, but could not be verified because the accumulation of particulate Mn(II) and Fe(II) – which represents the overwhelming fraction of the reduced pools – was not quantified. Here, we combined the indirect approach with independent determination of Mn and Fe reduction rates. Thus, we obtained two separate estimates of anaerobic carbon oxidation rates; based on DIC production and on the sum of sulfate, Fe, and Mn reduction converted to carbon equivalents, respectively (Table 4). At M1, within the 0–10 cm depth interval, the average ratio between total anaerobic C_{org} oxidation rate (10.7 mmol C m^{-2} d^{-1}) and the C_{org} oxidation from DIC production (14.0 mmol C m^{-2} d^{-1}) was 0.77 (Table 4). Similarly, at D3, the average ratio between total anaerobic C_{org} oxidation (6.79 mmol m^{-2} d^{-1}) and anaerobic DIC production (7.22 mmol m^{-2} d^{-1}) was 0.94. There was a good agreement between the two estimates with a ratio of total anaerobic C_{org} oxidation by Mn + Fe + sulfate: DIC production for individual depth intervals of 0.8–1.2 (Table 4) with the exception at the 0–2 cm depth of slope site (M1) where the ratio was slightly lower, 0.66, possibly due to a contribution from the C_{org} oxidation by nitrate reduction. The similarity of the two estimates across all incubations spanning a range of redox conditions provides confidence in our approach for calculating dissimilatory Mn and Fe reduction rates. Specifically, the good agreement indicates that the underlying assumptions concerning Mn adsorption and reactions of Fe(III) and sulfide are valid as first-order approximations. The general agreement further supports the validity of previous determinations of dissimilatory Mn and Fe reduction rates

based on the difference between DIC production and SO_4^{2-} reduction (Canfield et al., 1993a, 1993b; Thamdrup et al., 2000; Vandieken et al., 2006; Vandieken et al., 2014).

To elucidate the contribution of sulfate reduction in anaerobic carbon oxidation, the SRRs (Fig. 5B, 5G) were converted to carbon oxidation (Thamdrup and Canfield, 1996), and then compared to the DIC production rates from anoxic bag incubation (Fig. 5C, 5H). At the slope site (M1), the fraction of anaerobic C_{org} oxidation coupled to sulfate reduction increased with depth from 48 % at 0–2 cm, to 80 % at 8–10 cm (Table 4). Thus, the excess C_{org} oxidation in the upper layers should be coupled to other electron accepting processes. Indeed, the C_{org} oxidation by Fe reduction (0.96 mmol m^{-2} d^{-1}) accounted for most of the remaining anaerobic C_{org} oxidation (12–18 % of DIC production) at 0–8 cm depth, consistent with the distribution of Fe(III) decreasing from > 25 µmol cm^{-3} near the surface (Fig. 6, Table 4). Mn reduction was of minor importance at M1 because of the low content of Mn oxide (< 3 µmol cm^{-3}). Carbon oxidation coupled to aerobic respiration was estimated to 3.1 mmol m^{-2} d^{-1} corresponding to 18 % of the total aerobic + anaerobic oxidation, while the contributions of Fe and sulfate reduction to this total were 12 % and 50 %, respectively (Table 4). As mentioned above, nitrate reduction/denitrification may contribute part of the unexplained 19 % of carbon oxidation, but most of this imbalance likely reflects the combined uncertainties in the estimates of the individual pathways. Additionally, our partitioning of carbon oxidation pathways could be biased towards the anaerobic electron acceptors due to the use of the diffusive oxygen uptake (DOU) rather than total oxygen uptake (TOU), which will exceed DOU if bioirrigation is active (Glud, 2008). Bioirrigation was not determined at our sites, but the pore water profiles show no indication of strong irrigation (Fig. 2). An average DOU/TOU ratio of ~0.6 has been reported for sediments at 1.5–2.5 km depth (Glud, 2008). Using this ratio, and assuming that TOU is partitioned similarly as DOU between aerobic carbon oxidation and reoxidation, aerobic carbon oxidation would account for 25 %, while Fe and sulfate reduction would account for 11 % and 46 % of of carbon oxidation, respectively. This, the potential bias from using DOU is not expected to affect the ranking of electron acceptors by quantitative importance (SO_4^{2-} > O_2 > Fe(III)), and, as discussed further below, the partitioning of C_{org} oxidation at M1 falls within the range previously reported for continental margin sediments.

In contrast to M1, C_{org} oxidation by sulfate reduction at the basin site (D3) accounted for only a small fraction (< 11 %) of anaerobic C_{org} oxidation at 0–6 cm interval and it only dominated carbon oxidation at 8–10 cm (Fig. 5H, Table 4). Oxygen and NO_3^- were depleted

within 3.6 mm and 1 cm depth of the sediment surface, respectively (Fig. 5F), while Mn and Fe(III) oxides were abundant at 0–4 cm and 0–6 cm, respectively. Consistent with the abundance of electron acceptors, high rates of Mn and Fe reduction (Fig. 5I and 5J) implied Mn and Fe reduction as the most significant C_{org} oxidation pathways to 6 cm depth. At 0–2 cm depth, C_{org} oxidation by aerobic respiration and Mn reduction accounted for 53 % and 43 % of total C_{org} oxidation, respectively (Fig. 6). At 2–4 cm, Mn reduction accounted for 73 % of total C_{org} oxidation and 92 % of anaerobic C_{org} oxidation (Table 4, Fig. 6). Its importance decreased to 22 % at 4–6 cm due to lower Mn contents, while microbial Fe(III) reduction here contributed 51 %, and the partitioning of sulfate reduction increased to 11 % (Fig. 6). Consequently, the relative distributionof each C_{org} oxidation pathway with depth at D3 (Fig. 6) matched well with the depth distribution of the respective electron acceptors (Fig. 5F). Overall, within the 10 cm depth sediment interval, Mn and Fe reduction were the dominant C_{org} oxidation pathways comprising 45 % and 20 % of total carbon oxidation, respectively, at the Mn and Fe oxide-rich site in the center of the UB (Table 4). Correction for a potential underestimation of TOU, as discussed for M1, would reduce the contributions of Mn and Fe reduction slightly to 41 % and 18 %, respectively.

Despite the high Fe oxide content at 0–4 cm at D3 (Fig. 5F), no solid $Fe(II)_{(oxal)}$ accumulation was observed at this depth range (Fig. 4). This indicates that Fe(III) reduction may not occur under these Mn-oxide rich conditions. Indeed, using acombination of 16S rRNA-stable isotope probing and geochemical analysis in three manganese oxides-rich sediments including the UB, Vandieken et al. (2012) identified bacteria related to *Colwellia*, *Oceanospillaceae* and *Arcobacter* as acetate-oxidizing bacteria that potentially reduce manganese, whereas no known iron reducers were detected in the Mn-rich sediment. Similarly, Thamdrup et al. (2000), in Mn oxide- rich Black Sea sediment, found that the abundance of viable Fe-reducing bacteria in most probable number counts was low in comparison to Mn reducers and the addition of ferrihydrite did not stimulate Fe reduction, which implied that Fe reduction should be outcompeted by the Mn reduction process.

As manganese reduction is thermodynamically more favorable than iron and sulfate reduction, the Mn^{2+} liberation (Fig. 4) is likely resulted from dissimilatory Mn reduction. Nonetheless, Mn reduction estimated from the increase of Mn^{2+} at 0–4 cm interval at D3 (Fig. 4) could be due to oxidation of Fe^{2+} or sulfide. Fe^{2+} may readily react with Mn oxides (Myers and Nealson, 1988; Lovley and Phillips, 1988) by the reaction $2Fe^{2+} + MnO_2 + 4H_2O = Mn^{2+} + 2Fe(OH)_3 + 2H^+$. However, in the Mn oxide-rich sediment of the Skagerrak, Canfield et al.

(1993b) revealed that the addition of Ferrozine, a strong complexation agent for Fe^{2+}, had no inhibitory effect on the Mn^{2+} liberation, indicating that the chemical reaction of MnO_2 with Fe^{2+} generated by Fe reduction was not responsible for the accumulation of Mn^{2+}.

Despite the anoxic conditions and nitrate depletion during the bag incubation, Mn reduction rates at 0–2 cm depth (Fig. 5I) based on Mn^{2+} accumulation were substantially lower than the rates inferred from DIC accumulation (Fig. 5H). A similar discrepancy was previously observed for the uppermost part of the Mn reduction zone (Thamdrup et al., 2000), and is likely explained by particularly strong sorption of Mn^{2+} to fresh Mn oxide surfaces, which is not included in the adsorption coefficient used here. Low Mn^{2+} together with the rapid decrease of nitrate at 0–2 cm depth at D3 (Fig. 2F, 2G) also suggested that dissolved reduced manganese might act as a reducing agent for nitrate as it was suggested by Aller et al. (1998) in the Panama Basin and Mogollón et al. (2016) in the deep-sea sediment of the Clarion-Clierton fracture zone in the northeast equatirial Pacific.

Previous estimation of denitrification in 0–2 cm depth of the UB ranged from 0.01 to 0.17 mmol N m^{-2} d^{-1} (Lee, 2009), which is equivalent to a C_{org} oxidation of 0.013–0.213 mmol C m^{-2} d^{-1} using the stoichiometric equation of $4H^+ + 5CH_2O + 4NO_3^- = 5CO_2 + 2N_2 + 7H_2O$. Based on the average, the contribution of carbon oxidation by denitrification (0.11 mmol C m^{-2} d^{-1}) should be minor at the basin site (≤ 3 % of total C_{org} oxidation at 0–2 cm; ~1 % of integrated C_{org} oxidation). This is consistent with the general consensus that C_{org} oxidation by denitrification is of little importance in most marine sediments (Sørensen et al., 1979; Canfield et al., 1993a; Trimmer and Engström, 2011). Denitrification may be even further suppressed in Mn-rich sediments due to competitive inhibition from Mn reduction (Trimmer et al., 2013).

4.2 C_{org} oxidation dominated by manganese reduction in the UB

Microbial Fe reduction has been quantified directly in sediments of various coastal oceans (Gribsholt et al., 2003; Kostka et al., 2002a, 2002b; Hyun et al., 2007, 2009b) and indirectly in deeper continental margins (Thamdrup and Canfield, 1996; Jensen et al., 2003; Kostka et al., 1999). Earlier estimation from 16 different continental margin sediments indicated that Fe(III) reduction contributed 22 % on average to anaerobic carbon oxidation (Thamdrup, 2000). Thus, the contributions from Fe(III) reduction of 12 % and 20 % of anaerobic C_{org} oxidation onthe slope (M1) and in the basin (D3) of the UB (Table 4) fall in the range of the

549 previous indirect estimates.

550 Unlike Fe reduction, direct estimation of manganese reduction rates is not easy, mainly
551 because of the restriction of the process to a thin surface layer (Sundby and Silverberg, 1985),
552 the rapid reduction of manganese oxides with H_2S and Fe^{2+} (Postma, 1985; Burdige and
553 Nealson, 1986; Kostka et al., 1995; Lovley and Phillips, 1988), and the adsorption of Mn^{2+} to
554 Mn oxide surface (Canfield et al., 1993b). For that reason, only two studies, from the
555 Skagerrak and Black Sea, are available for direct comparison on the partitioning of Mn
556 reduction. The process has also been indicated to be of importance in the Panama Basin based
557 on diagenetic modeling (Aller, 1990) and at some Artic shelf sites where it was however not
558 quantified separately from Fe reduction (Vandieken et al., 2006; Nickel et al., 2008). Mn
559 reduction was responsible for over 90 % of total C_{org} oxidationat 600 m depth in the
560 Skagerrak (Canfield et al., 1993b), and accounted for 13–45 % of anaerobic C_{org} oxidation in
561 the Black Sea shelf sites at 60–130 m of water depth (Thamdrup et al., 2000). To our
562 knowledge, this report of C_{org} oxidation dominated by Mn reduction comprising 45 % of total
563 C_{org} oxidation and 57 % of anaerobic C_{org} respiration in the center of the UB (Table 4)
564 represents the first from deep-offshore basin of the eastern Asian marginal seas.

565 The difference in partitioning of Mn reduction in C_{org} oxidation between the UB, Black
566 Sea and Skagerrak reflects the close relationship between Mn oxide content in the sediment
567 and Mn reduction (Thamdrup et al., 2000). From the vertical distribution of electron
568 acceptors (Fig. 5F) and contribution of each C_{org} oxidation pathway with depth (Fig. 6), it is
569 apparent that the availability of Mn(IV) largely controls the relative contribution to C
570 oxidation. In the Skagerrak, the Mn oxides are abundant in high content down to 10 cm depth
571 (Canfield et al., 1993b), whereas Mn oxides in the Black Sea and the Ulleung Basin were
572 enriched only down to 2 cm and 4 cm, respectively (Thamdrup et al., 2000; Fig. 2G). Using
573 the available data set for the three marine sediments, we further plotted the relative
574 contribution of manganese reduction to anaerobic carbon oxidation as a function of Mn-
575 oxides content to expand data from Thamdrup et al., 2000 (Fig. 7). The plot indicates
576 saturation kinetics with a close correlation between Mn oxide content and the importance of
577 Mn reduction at low contents. Curve-fitting yields a content of MnO_2 at 50 % of contribution
578 of manganese reduction to total C_{org} oxidation (K_s) of 8.6 μmol cm^{-3} similar to the approx. 10
579 μmol cm^{-3} suggested before (Thamdrup et al., 2000). This indicates that Mn reduction can be
580 a dominant C_{org} oxidation process even at low contents of Mn oxides compared to those
581 found at UB. Manganese enrichments of this magnitude have been reported for several

582 locations on the continental margins and in deep basins (Murray et al., 1984; Gingele and
583 Kasten, 1994; Gobeil et al., 1997; Haese et al., 2000; Mouret et al., 2009; Magen et al., 2011;
584 Macdonald and Gobeil, 2012; Mewes et al., 2014) in addition to the relatively few places
585 where dissimilatory Mn reduction was already indicated to be of importance, as discussed
586 above. Thus, the process may be of more widespread significance, particularly in deep basin
587 settings such as UB that allow geochemical focusing of manganese.
588
589 **4.3 Source of high Mn oxide content**
590
591 The strong enrichment of Mn in the UB surface sediment is primarily of diagenetic origin as
592 indicated by just slightly higher Mn contents at depth in the sediment at D3 (mean 1.1 µmol
593 cm^{-3} at 10–20 cm depth) compared to M1 (0.45 µmol cm^{-3}) (Fig. 2) combined with higher
594 sediment accumulation rates at the slope (0.15–0.3 cm y^{-1}) than in the basin (0.07 cm y^{-1}; Cha
595 et al., 2005). Thus, the burial flux of Mn, and thereby the net input assuming steady state
596 deposition, is similar or higher at M1 compared to D3. Furthermore, Mn is likely subject to
597 geochemical focusing in the basin as Mn depositing at shallower depths is reductively
598 mobilized and incompletely oxidized in the thin oxic surface layer, resulting in release to the
599 water column and net down-slope transport, as inferred in other ventilated basins (Sundby
600 and Silverberg, 1985; Canfield at al., 1993b; Schaller and Wehrli, 1997). A diagenetic source
601 of Mn enrichment was also concluded in previous studies (Yin et al., 1989; Cha et al., 2007;
602 Choi et al., 2009). The Mn remaining and being buried at M1 likely represents unreactive
603 detrital forms to a larger extent than at D3 (Cha et al., 2007). Adopting the sediment
604 accumulation rate of 0.07 cm y^{-1} in the UB determined at a station 50 km from D3 (Cha et al.,
605 2005), the average $Mn_{(DCA)}$ content of 1.1 µmol cm^{-3} at 10–20 cm depth (Fig. 2G)
606 corresponds to a flux for permanent burial of 0.002 mmol m^{-2} d^{-1} or just 0.03 % of the Mn
607 reduction rate (Table 3), i.e., an Mn atom is recycled 3800 times before it finally gets buried
608 – first by stripping from the particles that settle to the seafloor and subsequently, over and
609 over, by reductive dissolution of the Mn oxides that from by reoxidation in the oxic surface
610 layer (or, potentially, in the nitrate zone; Aller et al., 1998; Mogollón et al., 2016). This is a
611 much more extensive recycling than found in the Mn sediment of Skagerrak (130–260 times;
612 Canfield et al., 1993b). The difference results mainly from a much higher burial flux of Mn
613 (as authigenic Mn[II]) in the Skagerrak (~40 µmol cm^{-3}; Canfield et al., 1993b). The reason
614 that little, if any, authigenic Mn(II) is buried in the UB is not clear.

As noted in previous studies (Aller, 1990; Canfield et al., 1993b), high contributions of Mn and Fe reduction to carbon oxidation in off-shore sediments requires physical mixing, which typically occurs through bioturbation. This is also the case for the UB, where the burial flux from the oxic surface layer into the Mn reduction zone corresponded to 0.4 mmol m^{-2} d^{-1} or 5 % of the Mn reduction rate (213 µmol cm^{-3} × 0.07 cm y^{-1}). Bioturbation has previously been inferred, but not quantified, from ^{210}Pb profiles in the UB (Cha, 2002), and thin polychaete worms were observed during our sampling. Assuming bioturbation to be a diffusive process, we estimate, in a similar manner as in the previous studies and based on the average gradient in $Mn_{(DCA)}$ from 0.5–1 to 7–8 cm, that the Mn reduction rate would be supported at a biodiffusion coefficient of 9.5 cm^2 y^{-1}. This value is 3.6 times lower than the coefficient estimated for the Skagerrak (Canfield et al., 1993b) and consistent with estimates for other sediments with similar deposition rates (Boudreau, 1994). Thus, it is realistic that bioturbation drives Mn cycling in the UB.

Meantime, the estimated biodiffusion coefficient of (Db) of 9.5 cm^2 yr^{-1} at Site D3 corresponds to ~2 % of the molecular diffusion coefficient of oxygen (388 cm^2 yr^{-1}). Judging from the absence of major fauna in the UB sediments, the mixing is brought about by small organisms with each individual affecting only a small area relative to the size of our cores, and the Db averaging many of these small but frequent events. Therefore, we see no contradiction between the presence of bioturbation and the relatively distinct redox zonation at D3 (Fig. 5F). Similarly, Hyacinthe et al. (2001) found that well defined profiles can be observed in both sediments with low and high bioactivity in the Bay of Biscay.

4.4 The UB as a biogeochemical hotspot

The SRRs measured in this study (0.43–4.29 mmol m^{-2} d^{-1}) are higher than those measured in productive systems such as the Benguela upwelling system in the Southeast Atlantic (0.14–1.39 mmol m^{-2} d^{-1}; Ferdelman et al., 1999), and even comparable to those reported at the Chilean (2.7–4.8 mmol m^{-2} d^{-1}; Thamdrup and Canfield, 1996) and Peruvian (5.2 mmol m^{-2} d^{-1}; Fossing, 1990) upwelling system at a similar depth range of 1000–2500 m. The total anaerobic DIC production rates at the slope (14.0 mmol m^{-2} d^{-1}) and basin site (7.2 mmol m^{-2} d^{-1}) were also comparable to those measured at the same depth range of a Chilean upwelling site (9.2–11.6 mmol m^{-2} d^{-1}) (Thamdrup and Canfield, 1996). Since rates of benthic carbon oxidation are largely controlled by the supply of organic carbon (Canfield et al., 2005), a high

organic carbon flux reflected in the high organic carbon content (> 2.5 %, dry wt.) in the sediment of the UB (Table 1) is likely to explain the high metabolic activities. A similar high organic carbon content as in the UB is rarely found in deep-sea sediment underlying oxic bottom water at depths exceeding 2000 m, except for a Chilean upwelling site (Lee et al., 2008). This high organic carbon content in the UB is mainly associated with the combination of enhanced biological production resulting from the formation of coastal upwelling (Hyun et al., 2009a), occurrence of an intrathermocline eddy resulting in the extraordinary subsurface chlorophyll-a maximum (Kim et al., 2012), high organic C accumulation rates exceeding 2 g C m^{-2} yr^{-1} (Lee et al., 2008), and high export production (Kim et al., 2009). In addition to the large vertical sinking flux, the lateral transport of the organic matter along the highly productive southeastern slope of the UB also contributes to the high organic carbon content (Lee et al., 2015). Consequently, high benthic mineralization resulting from the high organic content in the sediment implied that the UB is a biogeochemical hotspot where significant turnover of organic matter and nutrient regeneration occur.

Recent oceanographic observations revealed that the gradual deoxygenation and warming of the bottom water of the East Sea over the last 30 years have resulted in an ~10 % decrease in dissolved oxygen and ~0.04 ℃ increase in potential temperature (Kim et al., 2001; Gamo et al., 2011). Benthic metabolism and respiratory C_{org} oxidation coupled to various TEAP in the sediments are largely controlled by the combination of O_2 content, temperature and biological production overlying water column (Canfield et al., 2005). It is thus important to monitor any changes in the rates and partitioning of C_{org} oxidation to better understand and predict the variations of biogeochemical cycles of carbon, nutrients and metals potentially associated with long-term climatic changes in the UB, the biogeochemical hotspot of the East Sea.

5. Conclusions

Surface sediments of the Ulleung Basin (UB) in the East Sea are characterized by a high organic carbon content (> 2.5 %, dry wt.), high contents of Fe oxides (up to 100 μmol cm^{-3}), and very high contents of Mn oxides (> 200 μmol cm^{-3}). We show that microbial Mn and Fe reduction are the dominant C_{org} oxidation pathways, comprising 45 % and 20 % of total C_{org} oxidation, respectively. The high Mn content results from highly efficient recycling through reoxidation with very low permanent burial of authigenic Mn(II) phases. The basin

topography may ensure that any Mn^{2+} escaping to the overlying water returns to the sediment after reprecipitation. The relative importance of Mn reduction to C_{org} oxidation displays saturation kinetics with respect to Mn oxide content with a low half-saturation value (8.6 μmol cm^{-3}), which further implies that Mn reduction can be a dominant C_{org} oxidation process in sediments with lower MnO_2 content, and thereby that the process might be more important in continental margin and deep basin sediments than previously thought. Vertical distributions of the major terminal electron acceptors such as O_2, nitrate, Mn- and Fe oxides were systematically zonated with discrete sequential depletion according to the order of decreasing energy yield for C_{org} oxidation, which are not sharply separated in most aquatic sediments due to, e.g., sediment heterogeneity and mixing resulting from bioirrigation, bioturbation, and bottom turbidity currents. High benthic mineralization resulting from the high organic carbon content in the sediment implied that the UB is a biogeochemical hotspot where significant turnover of organic matter and nutrient regeneration occur.

Author contribution

J-H Hyun as first author and leader of the Korean research group designed the original experiments and conducted most writing; S-H Kim, J-S Mok, and H Cho participated in onboard research activities and analytical processes; V Vandieken participated in onboard research and was actively involved in the discussion of the manuscript; D Lee, as project manager of the EAST-1 program, paid the ship-time and has participated in discussion of the results; B Thamdrup, as leader of the Danish research group, collaborated with J-H Hyun in designing the experiments and writing and discussing the manuscript.

Acknowledgements

This research was a part of the projects titled Korean Long-term Marine Ecological Researches (K-LTMER) and East Asian Seas Time Series-II (EAST-II) funded by the Korean Ministry of Oceans and Fisheries, and was also supported by the National Research Foundation of Korea (NRF-2012-013-2012S1A2A1A01030760) in collaboration with the Danish Council for Independent Research and the Danish National Research Foundation (DNRF53).

712

713 **References**

714

715 Aller, R. C. : Bioturbation and manganese cycling in hemipelagic sediments, Phil. Trans. R.
716 Soc. Lond. A 331, 51-68, 1990.

717 Aller, R. C., Hall, P. O. J., Rude, P. D., and Aller, J. Y. : Biogeochemical heterogeneity and
718 suboxic diagenesis in hemipelagic sediments of the Panama Basin, Deep-Sea Res. I, 45,
719 133-165, 1998.

720 Belkin, I. M. : Rapid warming of Large Marine Ecosystems, Prog. Oceanogr., 81, 207-213,
721 2009.

722 Berg, P., Risgaard-Petersen, N., and Rysgaard, S. : Interpretation shelf and slope: A
723 comparison of *in situ* microelectrode and chamber flux measurements, Limnol. Oceanogr.,
724 37**,** 614-629, 1998.

725 Boudreau, B. P. : Is burial velocity a master parameter for bioturbation?, Geochim.
726 Cosmochim. Acta, 58, 1243-1249, 1994.

727 Bowles, M. W., Mogollón, J. M., Kasten, S., Zabel, M., and Hinrichs, K.U. : Global rates of
728 marine sulfate reduction and implications for sub-sea-floor metabolic activities, Science,
729 344, 889-891, 2014.

730 Broecker, W. S. : The great ocean conveyor, Oceanogr., 4, 79-89, 1991.

731 Broecker, W. S. and Peng, T. H. : Tracers in the sea, Lamont-Doherty Earth Observatory,
732 Palisades, NY., 1982.

733 Burdige, D. J.and Nealson, K. H. : Chemical and microbiological studies of sulfide-mediated
734 manganese reduction, Geomicrobiol. J., 4, 361-387, 1986.

735 Canfield, D. E., Jørgensen, B. B., Fossing, H., Glud, R., Gundersen, J., Rasing, N. B.,
736 Thamdrup, B., Hansen, J. W., Nielsen, L. P., and Hall, P. O. J. : Pathways of organic
737 carbon oxidation in three continental margin sediments, Mar. Geol., 113, 27-40, 1993a.

738 Canfield, D. E., Thamdrup, B., and Hansen, J. W. : The anaerobic degradation of organic
739 matter in Danish coastal sediments: iron reduction, manganese reduction, and sulfate
740 reduction, Geochim. Cosmochim. Acta, 57, 3867-3883, 1993b.

741 Canfield, D. E., Thamdrup, B., and Kristensen, E. (Eds.) : Aquatic geomicrobiology, Elsevier,
742 San Diego, 640 pp., 2005.

743 Cha, H. J., Choi, M. S., Lee, C.-B., and Shin, D.-H. : Geochemistry of surface sediments in
744 the southwestern East/Japan Sea, J. Asian Earth Sci., 29, 685-697, 2007.

745 Cha, H. J., Lee, C. B., Kim, B. S., Choi, M. S., and Ruttenberg, K. C. : Early diagenetic
746 redistribution and burial of phosphorus in the sediments of the southwestern East Sea
747 (Japan Sea), Mar. Geol., 216, 127-143, 2005.
748 Cha, H. J. : Geochemistry of surface sediments and diagenetic redistribution of phosphorus in
749 the southwestern East Sea, PhD thesis, Seoul National Univ., Seoul, Korea, 190 pp., 2002.
750 Choi, Y. J., Kim, D. S., Lee, T. H., and Lee, C. B. : Estimate of manganese and iron oxide
751 reduction rates in slope and basin sediments of Ulleung Basin, East Sea, J. Korean Soc.
752 Oceanogr., 14, 127-133, 2009.
753 Chough, S. K., Lee, H., J., and Yoon, S. H. (Eds.) : Marine Geology of Korean Seas (2nd
754 edition), Elsevier, Amsterdam, 2000.
755 Cline, J. D. : Spectrophotometric determination of hydrogen sulfide in natural waters, Limnol.
756 Oceanogr., 14, 454-458, 1969.
757 D'Hondt, S., Inagaki, F., Zarikian, C. A., Abrams, L. J., Dubois, N., Engelhardt, T., Evans,
758 H., Ferdelman, T., Gribsholt, B., Harris, R. N., Hoppie, B. W., Hyun, J.-H. et al. :
759 Presence of oxygen and aerobic communities from sea floor to basement in deep-sea
760 sediments, Nature Geosci, 8, 299-304, 2015.
761 Ferdelman, T. G., Fossing, H., Neumann, K., and Schulz, H. D. : Sulfate reduction in surface
762 sediments of the southeast Atlantic continental margin between 15°38´S and 27°57´S
763 (Angola and Namibia), Limnol. Oceanogr., 44, 650-661, 1999.
764 Fossing, H., Ferdelman, T. G., and Berg, P. : Sulfate reduction and methane oxidation in
765 continental margin sediments influenced by irrigation (South-East Atlantic off Namibia),
766 Geochim. Cosmochim. Acta, 64, 897-910, 2000.
767 Fossing, H. and Jørgensen, B. B. : Measurement of bacterial sulfate reduction in sediments:
768 evaluation of a single-step chromium reduction method, Biogeochem. 8, 205-222, 1989.
769 Froelich, P. N., Klinkhammer, G.P., Bender, M.L., Luedtke, N.A., Heath, G.R., Cullen, D.,
770 Dauphin, P., Hammond, D., Hartman, B., and Maynard, V. : Early oxidation of organic
771 matter in pelagic sediments of the eastern equatorial Atlantic: suboxic diagenesis,
772 Geochim. Cosmochim. Acta, 43, 1075-1090, 1979.
773 Gamo, T. : Dissolved oxygen in the bottom water of the Sea of Japan as a sensitive alarm for
774 global climatic change, Trend Anal.Chem., 30, 1308-1319, 2011.
775 Gamo, T., Nakayama, N., Takahata, N., Sano, Y., Zhang, J., Yamazaki, E., Taniyasu, S., and
776 Yamashita, N. : The Sea of Japan and its unique chemistry revealed by time-series
777 observations over the last 30 Year, Monogr. Environ. Earth Planets, 2, 1-22, 2014.

778 Gingele, F. X. and Kasten, S. : Solid-phase manganese in Southeast Atlantic sediments
779 Implications for the paleoenvironment, Mar. Geol., 121, 317-332, 1994.
780 Glud, R. N. : Oxygen dynamics of marine sediments, Mar. Biol. Res., 4, 243-289, 2008.
781 Gobeil, C, Macdonald, R. W.,and Sundby, B. : Diageneticseparation of cadmium and
782 manganese in suboxiccontinental margin sediments, Geochim. Cosmochim. Acta, 61,
783 4647-4654, 1997.
784 Gribsholt, B., Kostka, J. E., and Kristensen, E. : Impact of fiddler crabs and plant roots on
785 sediment biogeochemistry in a Georgia saltmarsh, Mar. Ecol. Prog. Ser., 259, 237-251,
786 2003.
787 Haese, R. R., Schramm, J., Rutgers Van Der Loeff, M. M., and Schulz, H. D. : A
788 comparativestudy of iron andmanganese diagenesis in continental slope and deep
789 seabasinsediments off Uruguay (SW Atlantic), Int. J. EarthSci., 88, 619-629, 2000.
790 Hall, P. O.and Aller, R.C. : Rapid small-volume, flow injection analysis for CO_2 and NH_4^+ in
791 marine and freshwaters, Limnol. Oceanogr., 37, 113-119, 1992.
792 Hansen, C., Zabel, M., and Schulz, H. N. : Benthic cycling of oxygen, nitrogen, and
793 phosphorus, in:Marine Geochemistry, edited by: Schulz, H. D.and Zabel, M., Springer-
794 Verlag, Berlin, Heidelberg, NY, 207-240, 2006.
795 Hansen, J. W., Thamdrup, B., and Jørgensen, B. B. : Anoxic incubation of sediment in gas-
796 tight plastic bags: a method for biochemical process studies, Mar. Ecol. Prog. Ser., 208,
797 273-282, 2000.
798 Hines, M. E., Bzylinski, D. A., Tugel, J. B., and Lyons, W. B. : Anaerobic microbial
799 biogeochemistry in sediments from two basins in the Gulf of Maine: evidence for iron and
800 manganese reduction, Estuar. Coast. Shelf Sci., 32, 313-324, 1991.
801 Hyacinthe, C., Anschutz, P., Carbonel, P., Jouanneau, J.-M., Jorissen, F.J. : Early diagenetic
802 processes in the muddy sediments of the Bay of Biscay, Mar. Geol., 177, 111–128, 2001.
803 Hyun, J.-H., Kim, D., Shin, C.-W., Noh, J.-H., Yang, E.-J., Mok, J.-S., Kim, S.-H., Kim, H.-
804 C., and Yoo, S. : Enhanced phytoplankton and bacterioplankton production coupled to
805 coastal upwelling and an anticyclonic eddy in the Ulleung basin, East Sea, Aquat. Microb.
806 Ecol., 54, 45–54, 2009a.
807 Hyun, J.-H., Mok, J.-S., Cho, H.-Y., Kim, S.-H., and Kostka, J. E. : Rapid organic matter
808 mineralization coupled to iron cycling in intertidal mud flats of the Han River estuary,
809 Yellow Sea, Biogeochem., 92, 231-245, 2009b.

Hyun, J.-H., Mok, J.-S., You, O.-R., Kim, D.,and Choi, D. L.: Variations and controls of sulfate reduction in the continental slope and rise of the Ulleung basin off the southeast Korean upwelling system in the East Sea, Geomicrobiol. J.,27, 1-11, 2010.

Hyun, J.-H., Smith, A. C., and Kostka, J. E. : Relative contributions of sulfate- and iron(III) reduction to organic matter mineralization and process controls in contrasting habitats of the Georgia saltmarsh, Appl. Geochem., 22, 2637-2651, 2007.

Jahnke, R. A., Reimers, C. E., and Craven, D. B. : Intensification of recycling of organic matter at the sea floor near ocean margins, Nature, 348, 50-54, 1990.

Jahnke, R. A.and Jahnke, D. B. : Rates of C, N, P and Si recycling and denitrification at the US mid-Atlantic continental slope depocenter, Deep-Sea Res. I, 47, 1405-1428, 2000.

Jahnke,R. A., Emerson, S. R., and Murray, J. W. : A model of oxygen reduction, denitrification, and organic matter mineralization in marine sediments, Limnol. Oceanogr., 27, 610-623, 1982.

Jensen, M. M., Thamdrup, B., Rysgaard, S., Holmer, M., and Fossing, H. : Rates and regulation of microbial iron reduction in sediments of the Baltic–North Sea transition, Biogeochem., 65, 295-317, 2003.

Jørgensen, B. B. and Kasten, S. : Sulfur cycling and methane oxidation. in: Marine Geochemistry, edited by: Schulz, H. D. and Zabel, M., Springer-Verlag, Berlin, Heidelberg, NY, 271-309, 2006.

Jørgensen, B. B. : A comparison of methods for the quantification of bacterial sulfate reduction in coastal marine sediments, 1. Measurement with radiotracer techniques, Geomicrobiol. J., 1, 11–28, 1978.

Jørgensen, B. B. : Bacteria and marine biogeochemistry,in:Marine Geochemistry, edited by: Schulz, H. D.and Zabel, M., Springer-Verlag, Berlin, Heidelberg, NY, 169-206, 2006.

Jørgensen, B. B. : Mineralization of organic matter in the sea bed - the role of sulphate reduction, Nature, 296, 643-645, 1982.

Jørgensen, B. B.and Revsbech, N. P. : Diffusive boundary layers and the oxygen uptake of sediments and detritus, Limnol. Oceanogr., 30, 111-122, 1985.

Kang, D. J., Lee, D. S., and Kim, K.-R. : The East Sea (Sea of Japan), in:Carbon and nutriet fuxes in continental margins, edited by: Liu, K.-K., Atkinson, L., Quiñones, R. A., and Talaue-MaManus, L., Springer-Verlag, Berlin, Heidelberg, 383-394, 2010.

Kim K, Kim K.-R., Min, D. H., Volkov, Y., Yoon, J.-H., Takematsu, M. : Warming and structural changes in the East Sea (Japan) Sea: a clue to future changes in the global

oceans?, Geophys. Res. Lett., 28, 3293-3296, 2001.

Kim, D., Choi, M.-S., Oh, H.-Y., Kim, K. H., and Noh, J.-H. : Estimate of particulate organic carbon export flux using $^{234}Th/^{238}U$ disequilibrium in the southwestern East Sea during summer, (The Sea) J. Kor. Soc. Oceanogr., 14, 1-9, 2009.

Kim, D., Yang, E.J., Kim, K. H., Shin, C.-W., Park, J., Yoo, S. J., and Hyun, J.-H. : Impact of an anticyclonic eddy on the summer nutrient and chlorophyll a distributions in the Ulleung Basin, East Sea (Japan Sea),ICES J. Marine Science, 69, 23-29, 2012.

Kostka, J. E., Gribsholt, B., Petrie, E., Dalton, D., Skelton, H., and Kristensen, E. : The rates and pathways of carbon oxidation in bioturbated saltmarsh sediments, Limnol.Oceanogr., 47, 230-240, 2002a.

Kostka, J. E., Roychoudhury, A., and Van Cappellen, P. : Rates and controls of anaerobic microbial respiration across spatial and temporal gradients in saltmarsh sediments, Biogeochem, 60, 49–76, 2002b.

Kostka, J. E., Thamdrup, B., Glud, R. N., and Canfield, D. E. : Rates and pathways of carbon oxidation in permanently cold Arctic sediments, Mar. Ecol. Prog. Ser., 180, 7-21, 1999.

Kostka, J. E., Luther, G. W., and Nealson, K. H. : Chemical and biological reduction of Mn(III)-pyrophosphate complexes – potential importance of dissolved Mn(III) as an environmental oxidant, Geochim. Cosmochim. Acta, 59, 885-894, 1995.

Lee, J. S., An, S.-U., Park, Y.-G., Kim, E., Kim, D., Kwon, J. N., Kang, D.-J., and Noh, J.-H. : Rates of total oxygen uptake of sediments and benthic nutrient fluxes measured using an in situ autonomous benthic chamber in the sedimentof the slope off the southwestern part of the Ulleung Basin, East Sea, Ocean Sci. J., 50, 581-588, 2015.

Lee, J.: Importance of nitrate reduction in coastal and deep-sea sediments, MS thesis, Department of Marine Science Graduate School, Pusan National University, Korea, 86 pp., 2009.

Lee, T., Hyun, J.-H., Mok, J. S., and Kim, D. : Organic carbon accumulation and sulfate reduction rates in slope and basin sediments of the Ulleung basin, East/Japan Sea, Geo. Mar. Lett. 28, 153-159, 2008.

Li, Y. H.and Gregory, S. : Diffusion of ions in sea water and deep sea sediments. Geochim. Cosmochim. Acta, 38, 703-714, 1974.

Liu, K.-K., Atkinson, L., Quiñones, R. A., and Talaue-MaManus, L. : Biogeochemistry of the continental margins, in: Carbon and nutriet fuxes in continental margins, edited by: Liu, K.-K., Atkinson, L., Quiñones, R. A., and Talaue-MaManus, L., Springer-Verlag, Berlin,

876 Heidelberg, 3-24, 2010.
877 Lovley, D. R.and Phillips, E. J. P. : Competitive mechanisms for inhibition of sulfate
878 reduction and methane production in the zone of ferric iron reduction in sediments, Appl.
879 Environ. Microbiol., 53, 2636-2641, 1987.
880 Lovley, D. R.and Phillips, E. J. P. : Manganese inhibition of microbial iron reduction in
881 anaerobic sediments, Geomicrobiol.J., 6, 145-155, 1988.
882 Luther III, G. W. : Acid volatile sulfide – A comment, Mar. Chem., 97, 198-205, 2005.
883 Macdonald, R. W. and Gobeil, C. : Manganese sources andsinks in the Arctic Oceanwith
884 reference to periodicenrichments in basin sediments, Aquat. Geochem., 18, 565-591, 2012.
885 Madison, S., Tebo, B. M., Mucci, A., Sundby, B., and Luther III, G. W. : Abundant
886 porewater Mn(III) is a major component of the sedimentary redox system, Science, 341,
887 875-878, 2013.
888 Magen, C., Mucci, A., and Sundby, B. : Reduction rates of sedimentary Mn and Fe oxides: an
889 incubation experiment with Arctic Ocean sediments, Aquat. Biogeochem., 17, 629-643,
890 2011.
891 Melton, E. D., Swanner, E. D., Behrens, S., Schmidt, C., and Kappler, A. : The interplay of
892 microbially mediated and abiotic reactions in the biogeochemical Fe cycle, Nature Rev.
893 Microbiol., 12, 797-808, 2014.
894 Mewes, K., Mogollón, J. M., Picard, A., Rühlemann, C., Eisenhauer, A., Kuhn, T., Ziebis, W.,
895 and Kasten, S. : Diffusive transfer of oxygen from seamount basaltic crust into overlying
896 sediments: an example from the Clarion-Clipperton Fracture Zone, Earth Planet. Sci. Lett.,
897 433, 215-225, 2016.
898 Mewes, K., Mogollón, J. M., Picard, A., Rühlemann, C., Kuhn, T., Nöthen, K., and Kasten,
899 S. : Impact of depositional and biogeochemical processes on small scale variations in
900 nodule abundance in the Clarion-Clipperton Fracture Zone, Deep-Sea Res. I, 91, 125-141,
901 2014.
902 Meyers, C.and Nealson, K. H.: Microbial reduction of manganese oxides: Interactions with
903 iron and sulfur, Geochim. Cosmochim. Acta, 52, 2727-2732, 1988.
904 Mogollón, J. M., Mewes, K., and Kasten, S. : Quantifying manganese and nitrogen cycle
905 coupling in manganese-rich, organic carbon-starved marine sediments: examples from the
906 Clarion-Clipperton fracture zone, Geophys. Res. Lett., 43, doi:10.1002/2016GL069117,
907 2016.
908 Mouret, A., Anschutz, P., Lecroart, P., Chaillou, G., Hyacinthe, C.,Deborde, J., Jorissen,

F.,Deflandre, B., Schmidt, S.,and Jouanneau, J.-M. : Benthic geochemistry of manganese inthe Bayof Biscay, and sediment mass accumulation rate, Geo. Mar. Lett. 29, 133-149, 2009.

Murray, J. W., Balistrieri, L. S., and Paul, B. : The oxidation stateof manganese in marinesediments and ferromanganesenodules, Geochim. Cosmochim. Acta, 48, 1237-1247, 1984.

Nickel, M., Vandieken, V., Brüchert, V., and Jørgensen, B. B. : Microbial Mn(IV) and Fe(III) reduction in northern Barents Sea sediments under different conditions of ice cover and organic carbon deposition, Deep-Sea Res. II, 55, 2390-2398, 2008.

Parsons, T. R., Maita, Y., and Lalli, C. M.(Eds.) : A manual of chemical and biological methods for seawater analysis, Pergamon Press, Oxford, 173 pp., 1984.

Phillips, E. J. P.and Lovley, D. R. : Determination of Fe(III) and Fe(II) in oxalate extracts of sediment, Soil Sci. Soc. Am. J., 51, 938-941, 1987.

Postma, D. : Concentration of Mn and separation from Fe in sediments – I. Kinetics and stoichiometry of the reaction between birnessite and dissolved Fe(II) at 10^{o}C, Geochim. Cosmochim. Acta, 49, 1023-1033, 1985.

Pyzik, A. E.and Sommer, S. E. : Sedimentary iron monosulfide: kinetics and mechanisms of formation, Geochim. Cosmochim. Acta, 45, 687-698, 1981.

Rasmussen, H. and Jørgensen, B. B. : Microelectrode studies of seasonal oxygen uptake in a coastal sediment: role of molecular diffusion, Mar. Ecol. Prog. Ser., 81, 289-303, 1992.

Rickard, D. and Morse, J. W. : Acid volatile sulfur (AVS), Mar. Chem., 97, 141-107, 2005.

Romankevich, E. A. : Geochemistry of organicmatter in the ocean,Springer-Verlag, Berlin, Heidelberg, NY, Tokyo, 334 pp., 1984.

Schaller, T. and Wehrli, B. : Geochemical-focusing of manganese in lake sediments –An indicator of deep-water oxygen conditions, Aqut. Geochem., 2, 359-378, 1997.

Slomp, C. P., Mort, H. P., Jilbert, T., Reed, D. C., and Gustafsson, B. G. : Coupled dynamics of iron and phosphorus in sediments of an oligotrophic coastal bsin and the impact of anaerobic oxidation of methane, PLoS ONE, 8, e62386, 2013.

Sørensen, J. W. and Jørgensen, B. B. : Early diagenesis in sediments from Danish coastal waters: Microbial activity and Mn-Fe-S geochemistry, Geochim. Cosmochim. Acta, 51, 1583-1590, 1987.

Sørensen, J. W., Jørgensen, B. B., and Revsbech, N. P. : A comparison of oxygen, nitrate and sulfate respiration in a coastal marine sediment, Microb. Ecol., 5, 105-115, 1979.

942 Stookey, L. L. : Ferrozine - a new spectrophotometric reagent for iron, Anal. Chemi. 42, 779-
943 781, 1970.
944 Sundy, B. and Silverberg, N. : Manganese fluxes in the benthic boundary layer, Limnol.
945 Oceanogr., 30, 372-381, 1985.
946 Thamdrup, B. and Canfield, D. E. : Pathways of carbon oxidation in continental margin
947 sediments off central Chile, Limnol. Oceanogr. 41, 1629-1650, 1996.
948 Thamdrup, B. and Dalsgaard, T. : The fate of ammonium in anoxic manganese oxide-rich
949 marine sediment, Geochim. Cosmochim. Acta, 64, 4157-4164, 2000.
950 Thamdrup, B., Rosselló-Mora, R., and Amann, R. : Microbial manganese and sulfate
951 reduction in Black Sea shelf sediments, Appl. Environ. Microbiol., 66, 2888-2897, 2000.
952 Thamdrup, B. : Bacterial manganese and iron reduction in aquatic sediments, Adv. Microb.
953 Ecol. 16, 41-84, 2000.
954 Trimmer, M. and Engström, P. : Distribution, activity, and ecology of anammox bacteria in
955 aquatic environments, in: Nitrification, edited by: Ward, B. B., Arp, D. J., and Klotz, M. G.,
956 ASM Press, Washington, DC, 201-235, 2011.
957 Trimmer, M., Engström, P., and Thamdrup, B. : Stark contrast in denitrification and anammox
958 across the deep Norwegian Trench in the Skagerrak, Appl. Environ. Microbiol., 79, 7381-
959 7389, 2013.
960 Vandieken, V, Pester, M., Finke, N., Hyun, J.-H., Friedrich, M. W., Loy, A., and Thamdrup,
961 B. : Identification of acetate-oxidizing manganese-reducing bacteria in three manganese
962 oxide-rich marine sediments by stable isotope probing, ISME J., 6, 2078-2090, 2012.
963 Vandieken, V., Finke, N., and Thamdrup, B. : Hydrogen, acetate, and lactate as electron
964 donors for microbial manganese reduction in a manganese-rich coastal marine sediment,
965 FEMS Micribiol Ecol., 87, 733-745, 2014.
966 Vandieken, V., Nickel, M., and Jørgensen, B. B. : Carbon mineralization in Arctic sediments
967 northeast of Svalbard: Mn(IV) and Fe(III) reduction as principal anaerobic respiratory
968 pathways, Mar. Ecol. Prog. Ser., 322, 15-27, 2006.
969 Walsh, J. J. : Importance of continental margins in the marine biogeochemical cycling of
970 carbon and nitrogen, Nature, 350, 53-55, 1991.
971 Yamada, K., Ishizaka, J., and Nagata, H. : Spatial and temporal variability of satellite primary
972 production in the Japan Sea from 1998 to 2002, J. Oceanogr., 61, 857-869, 2005.
973 Yin, J. H., Kajiwara, Y., and Fujii, T. : Distribution of transition elements in surface
974 sediments of the southwestern margin of Japan Sea. Geochem. J., 23, 161-180, 1989.

975 Yoo, S. and Park, J. S. : Why is the southwest the most productive region of the East Sea/Sea
976 of Japan?, J. Mar. Syst., 78, 301-315, 2009.

977

978 Table 1. Environmental settings and sediment characteristics

Environmental parameter	M1 (Continental slope)	D3 (Center of the basin)
Latitude	36° 10’ N	37° 00’ N
Longitude	130° 10’ E	131° 00’ E
Water depth (m)	1,453	2,154
Sediment temperature (^{o}C)	1.3	0.6
Pore-water salinity (psu)	34.2	34.8
Water content (%)	85 (± 3.1)	77 (± 1.8)
Porosity	0.95 (± 0.03)	0.86 (± 0.01)
Density (g cm^{-3})	1.10 (± 0.02)	1.12 (± 0.02)
Total organic carbon (%, dry wt.)	3.96 (± 0.27)	2.66 (± 0.09)
Total organic nitrogen (%, dry wt.)	0.38 (± 0.01)	0.35 (± 0.01)

979 Numbers in parenthesis indicate ± 1SD of triplicate samples.

980

981

Table 2. Oxygen penetration depth (OPD), diffusive oxygen utilization (DOU) rate and O_2 consumption rate by aerobic respiration and re-oxidation of reduced inorganic compounds (RIC) in the pore water.

Station	OPD (mm)	DOU (mmol O_2 m^{-2} d^{-1})	O_2 consumption (mmol O_2 m^{-2} d^{-1}) by	
			Aerobic respiration	Re-oxidation of RIC
M1	3.2 (± 0.20)	7.12 (± 1.36)	4.04 (± 2.03)	3.07 (± 0.68)
D3	3.6 (± 0.03)	5.95 (± 0.16)	2.53 (± 0.72)	3.42 (± 0.58)

Values represent averages ± 1SD (n = 3)

Table 3. Depth integrated rates (mmol m^{-2} d^{-1}) of Mn reduction, Fe reduction, and sulfate reduction and the partitioning of abiotic and microbial Fe(III) reduction in total Fe(III) reduction with depth.

St.	Depth Interval (cm)	SO_4^{2-} Red	Mn Red	[a]Total Fe(III) Red	Fe reduction by		Fe $Red_{(Microbial)}$ / Fe $Red_{(Abiotic)}$
					[a]Abiotic Fe Red	[a]Microbial Fe Red	
M1	0–2	1.35	0.04	4.75	0.90	3.86	4.28
	2–4	1.04	-	3.02	0.70	2.33	3.33
	4–6	0.84	-	1.58	0.56	1.21	2.16
	6–8	0.54	-	1.25	0.36	0.89	2.47
	8–10	0.53	-	0.77	0.36	0.41	1.14
	Sum (0-10)	4.30	0.04	11.4	2.88	8.70	
D3	0–2	0.06	[b]3.19	-	-	-	n.a.
	2–4	0.11	3.96	1.63	0.07	1.56	22.3
	4–6	0.13	1.05	4.80	0.09	4.71	52.3
	6–8	0.06	0.01	0.86	0.04	0.83	20.8
	8–10	0.07	0.00	0.24	0.05	0.19	3.80
	Sum (0-10)	0.43	8.21	7.53	0.25	7.29	

[a]Stoichiometric equations were used to evaluate the relative significance of abiotic and microbial Fe reduction:
Abiotic reduction of Fe(III) by sulfide oxidation, $3H_2S + 2FeOOH = 2FeS + S^o + 4H_2O$; Microbial Fe(III) reduction = Total Fe(III) reduction – abiotic Fe(III) reduction.
[b]back-calculated from the C oxidation by Mn reduction in the 0–2 cm interval in Table 4 using the stoichiometric equation, $2MnO_2 + CH_2O + H_2O = 2Mn^{2+} + HCO_3^- + 3OH^-$.
' – ' indicates that the process does not occur or is regarded as negligible at the depth interval based on the OPD for aerobic respiration and geochemical profiles or anoxic bag incubations for Mn(IV) and Fe(III) reduction
'n.a.' indicates that data are not available.

Table 4. Organic carbon (C_{org}) oxidation (mmol C m^{-2} d^{-1}) by each C_{org} oxidation pathway, and its partitioning in total C_{org} oxidation (% Total C_{ox}) and anaerobic C_{org} oxidation (% Anaerobic C_{org} ox) at each depth interval within 10 cm of the sediment. Mn Red, Mn reduction; Fe Red, Fe reduction; and SO_4^{2-} Red, sulfate reduction

St.	Depth Interval (cm)	C_{org} oxidation measured by		[c]Total C_{org} oxidation (DOU + DIC)	Anaerobic C_{org} oxidation by dissimilatory			Total anaerobic C_{org} oxidation (Mn Red + Fe Red + SO_4^{2-} Red)	Total Anaerobic C_{org} oxidation / Anoxic DIC production
		[a]DOU (Aerobic respiration)	[b]DIC prod. (Anaerobic respiration)		[d]Mn Red	[d,e]Fe Red	[d]SO_4^{2-} Red		
M1	0–2	3.11	5.59	8.70	0.02	0.96	2.69	3.67	0.66
	2–4	-	3.31	3.31	-	0.58	2.09	2.67	0.81
	4–6	-	2.26	2.26	-	0.26	1.67	1.93	0.85
	6–8	-	1.50	1.50	-	0.22	1.08	1.30	0.87
	8–10	-	1.37	1.37	-	0.10	1.06	1.17	0.85
	Sum (0–10)	3.11	14.0	17.1	0.02	2.13	8.59	10.7	0.77
	(% Total C_{org} ox)	(18.1)	(81.9)	(100)	(0.13)	(12.4)	(50.1)	(62.7)	
	(% Anaerobic C_{org} ox)				(0.16)	(15.2)	(61.2)		
D3	0–2	1.94	1.72	3.66	[f]1.59	-	0.13	1.72	1.00
	2–4	-	2.72	2.72	1.98	0.39	0.22	2.58	0.95
	4–6	-	2.32	2.32	0.52	1.18	0.26	1.96	0.84
	6–8	-	*0.30*	0.30	0.01	0.21	0.12	0.33	1.10
	8–10	-	*0.16*	0.16	-	0.05	0.15	0.19	1.21
	Sum (0–10)	1.94	*7.22*	9.2	4.10	1.82	0.86	6.79	0.94
	(% Total C_{org} ox)	(20.6)	(78.8)	(100)	(44.8)	(19.9)	(9.41)	(77.8)	
	(% Anaerobic C_{org} ox)				(56.8)	(25.2)	(11.9)		

[a] Aerobic C_{org} oxidation rate (= O_2 consumption by aerobic respiration × (106C/138O_2) calculated using the Redfield ratio; O_2 consumption by aerobic respiration rate (= DOU - re-oxidation rates) is calculated from Table 2 that is derived from the O_2 micro-profiles in Fig. 2.

[b] independently measured from the DIC accumulation rate in anoxic bag incubation experiment in Fig. 4.

[c] Total C_{org} oxidation = aerobic C_{org} oxidation + anaerobic C_{org}.oxidation

[d] C_{org} oxidation by dissimilatory Mn(IV) reduction, Fe(III) reduction, and sulfate reduction was calculated from the stoichiometric equations: $2MnO_2 + CH_2O + H_2O = 2Mn^{2+} + HCO_3^- + 3OH^-$; $4Fe(OH)_3 + CH_2O = 4Fe^{2+} + HCO_3^- + 7OH^-$; $SO_4^{2-} + 2CH_2O = H_2S + 2HCO_3^-$, $H_2S = HS^- + H^+$

[e] Dissimilatory Fe(III) reduction = (Total Fe(III) reduction in Fig.5) – (Abiotic Fe(III) reduction coupled to H_2S oxidation; $3H_2S + 2FeOOH = 2FeS + S^o + 4H_2O$)

[f] back-calculated from: DIC production rate - (C oxidation by SO_4^{2-} Red and Fe Red). See text for further discussion

' – ' indicates that the process does not occur or is regarded as negligible based on the OPD for aerobic respiration and geochemical profiles or anoxic bag incubations for Mn and Fe Red.

Figure legends

Fig. 1. Sampling stations in the East Sea and pictures showing contrasting colors between surface sediments of the continental slope (M1) and center of the basin (D3)

Fig. 2. Concentrations of dissolved NH_4^+, NO_3^-, Mn^{2+} and Fe^{2+} in pore water and contents of solid phase $Mn_{(DCA)}$, $Fe(II)_{(oxal)}$, $Fe(III)_{(oxal)}$, acid volatile sulfur (AVS) and chromium reducible sulfur (CRS) in the sediment at M1 and D3.

Fig. 3. Vertical profiles of O_2. The slashed area indicates the diffusive boundary layer in the sediment-water interface. The shaded area indicates that O_2 consumption by aerobic respiration (I and II) and re-oxidation of reduced inorganic compounds (III), respectively.

Fig. 4. Changes of concentrations of DIC, Ca^{2+} and Mn^{2+} in pore water and contents of solid phase $Fe(II)_{(oxal)}$ during anoxic bag incubations of sediments from 0-2, 2-4, 4-6, and 6-8 cm depth at M1 and D3. Data obtained at 8-10 cm depth interval is not shown.

Fig. 5. Vertical distribution of terminal electron acceptors (O_2, NO_3^-, Mn and Fe) and rates of sulfate reduction measured from whole core analyses, and rates of anaerobic carbon oxidation (DIC production rates), Mn reduction and Fe reduction measured from anoxic bag incubations in Fig. 4. C_{org} by sulfate reduction in panel C and H was calculated from the stoichiometry of 2:1 of C_{org} oxidized to sulfate reduced.

Fig. 6. Depth variations of partitioning of each carbon oxidation pathway in total carbon oxidation at M1 and D3

Fig. 7. The relative contribution of Mn reduction to anaerobic carbon oxidation as a function of the content of Mn(DCA) at 3 different sites. BS, Black Sea (Thamdrup et al. 2000); UB, Ulleung Basin (This study); Sk, Skagerrak (Canfield et al. 1993b).

Hyun et al. – Figure 1

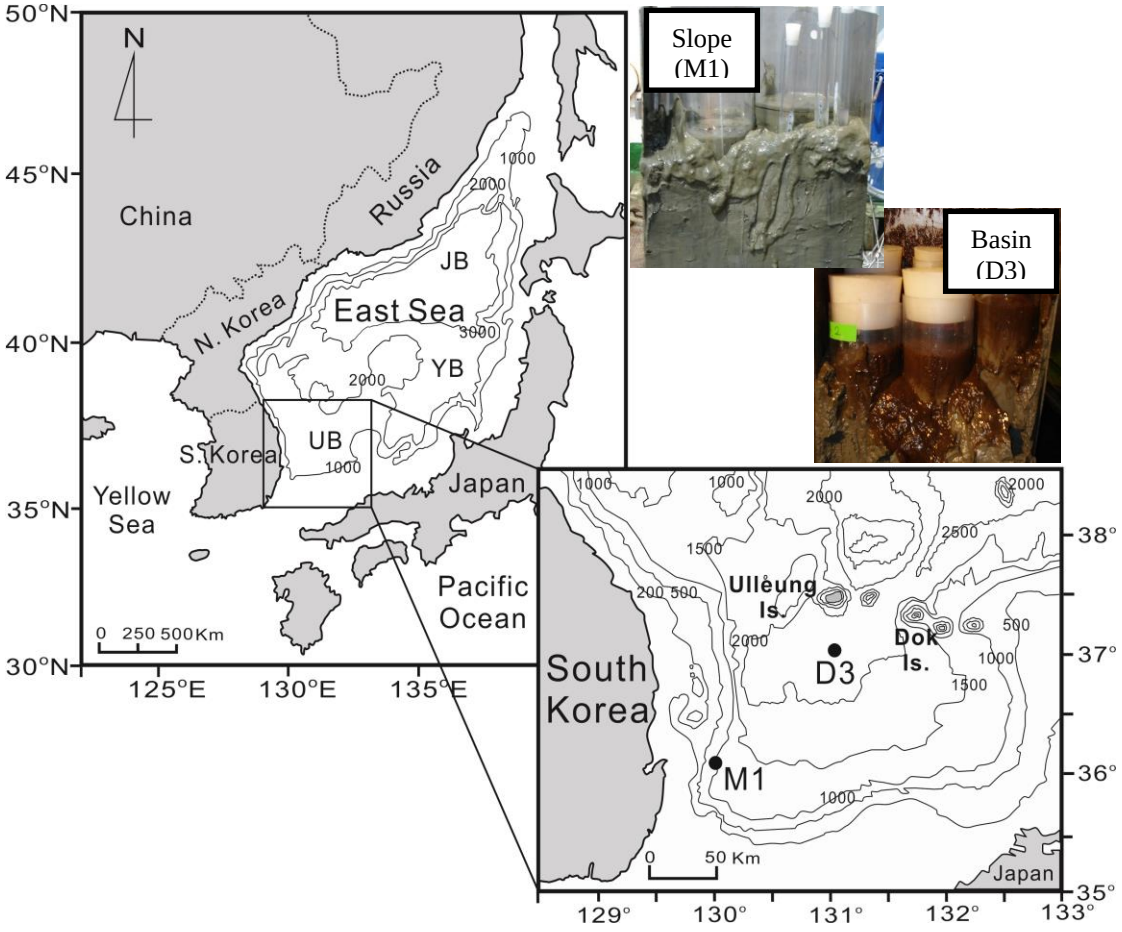

1 Hyun et al – Figure 2

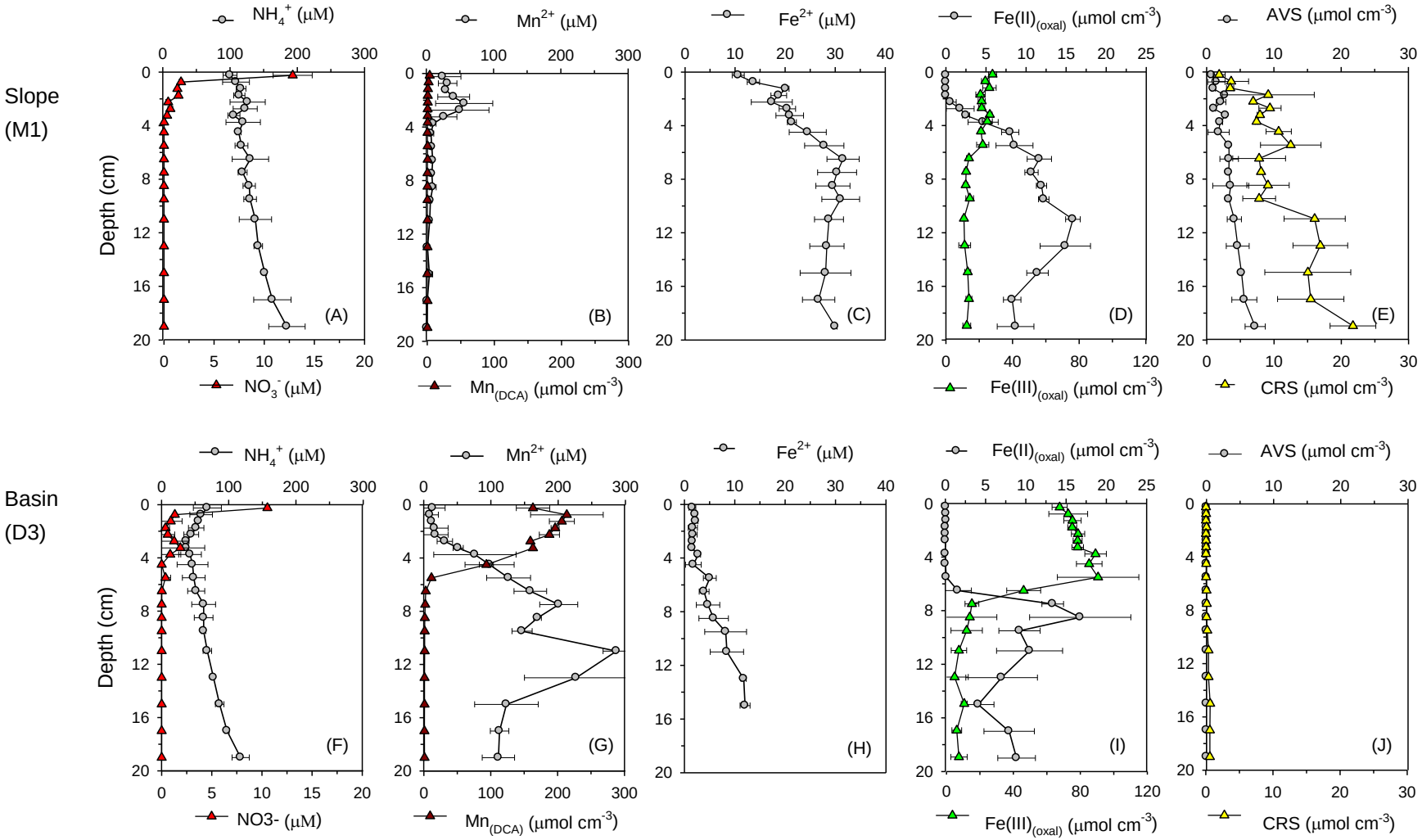

2

Hyun et al – Figure 3

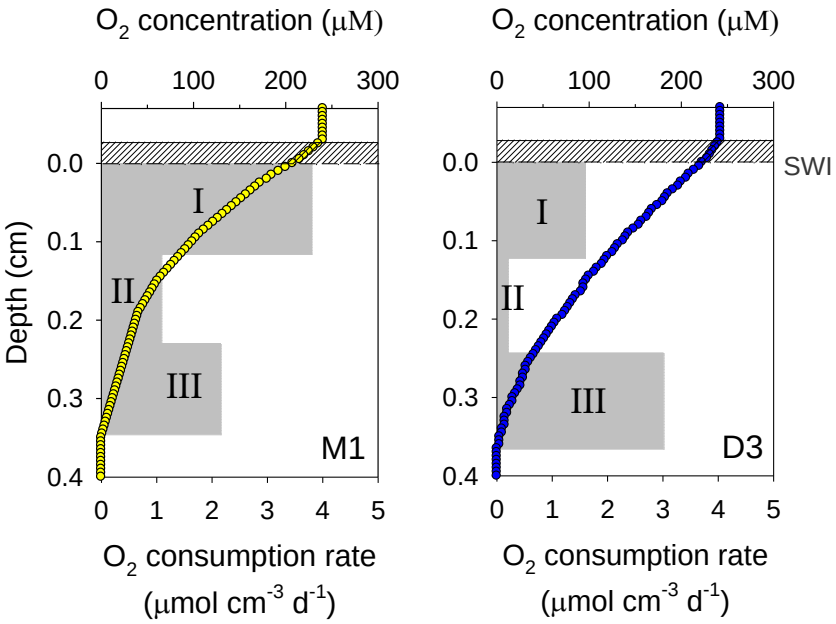

14 Hyun et al – Figure 4

15

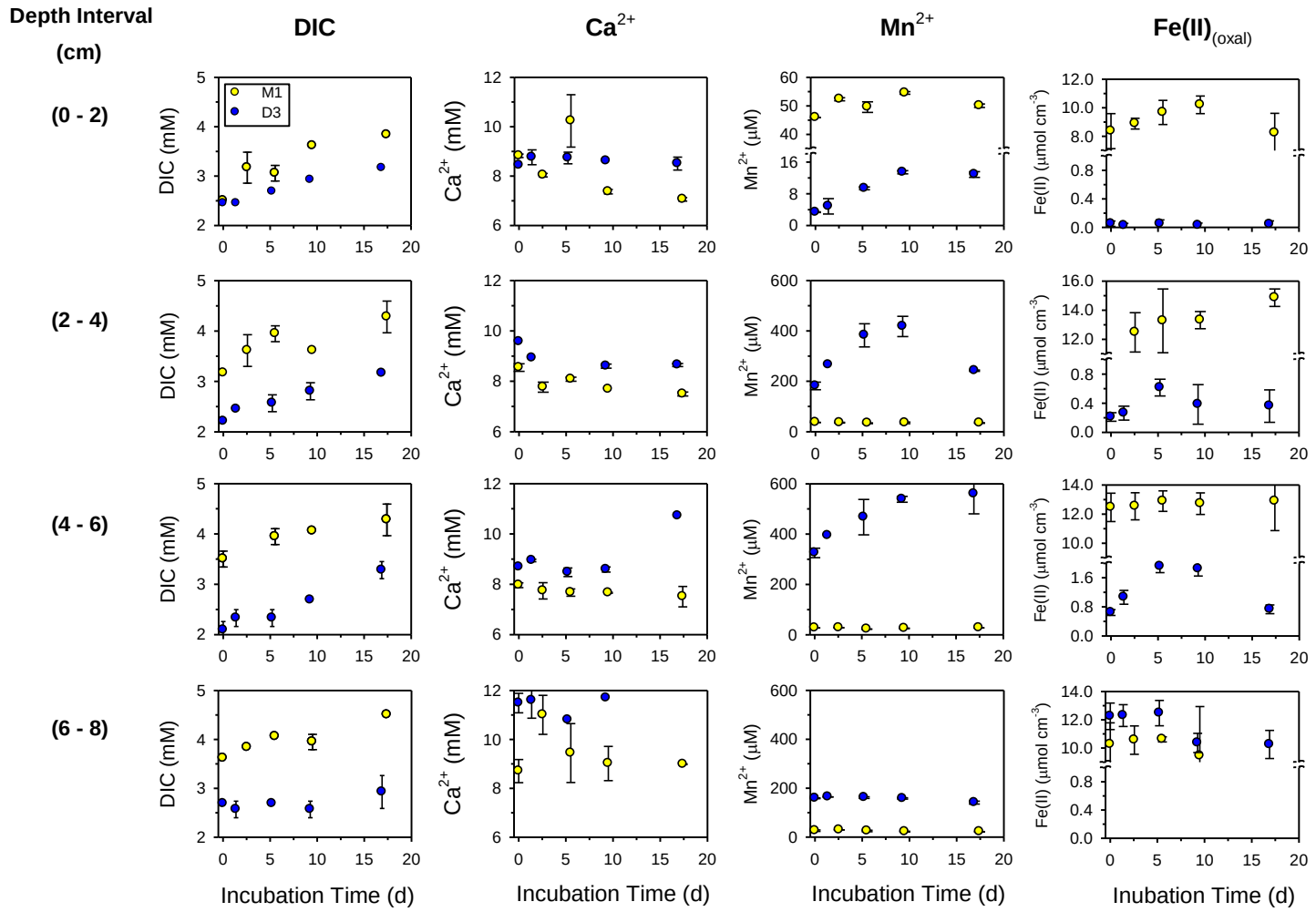

16

Hyun et al. – Figure 5

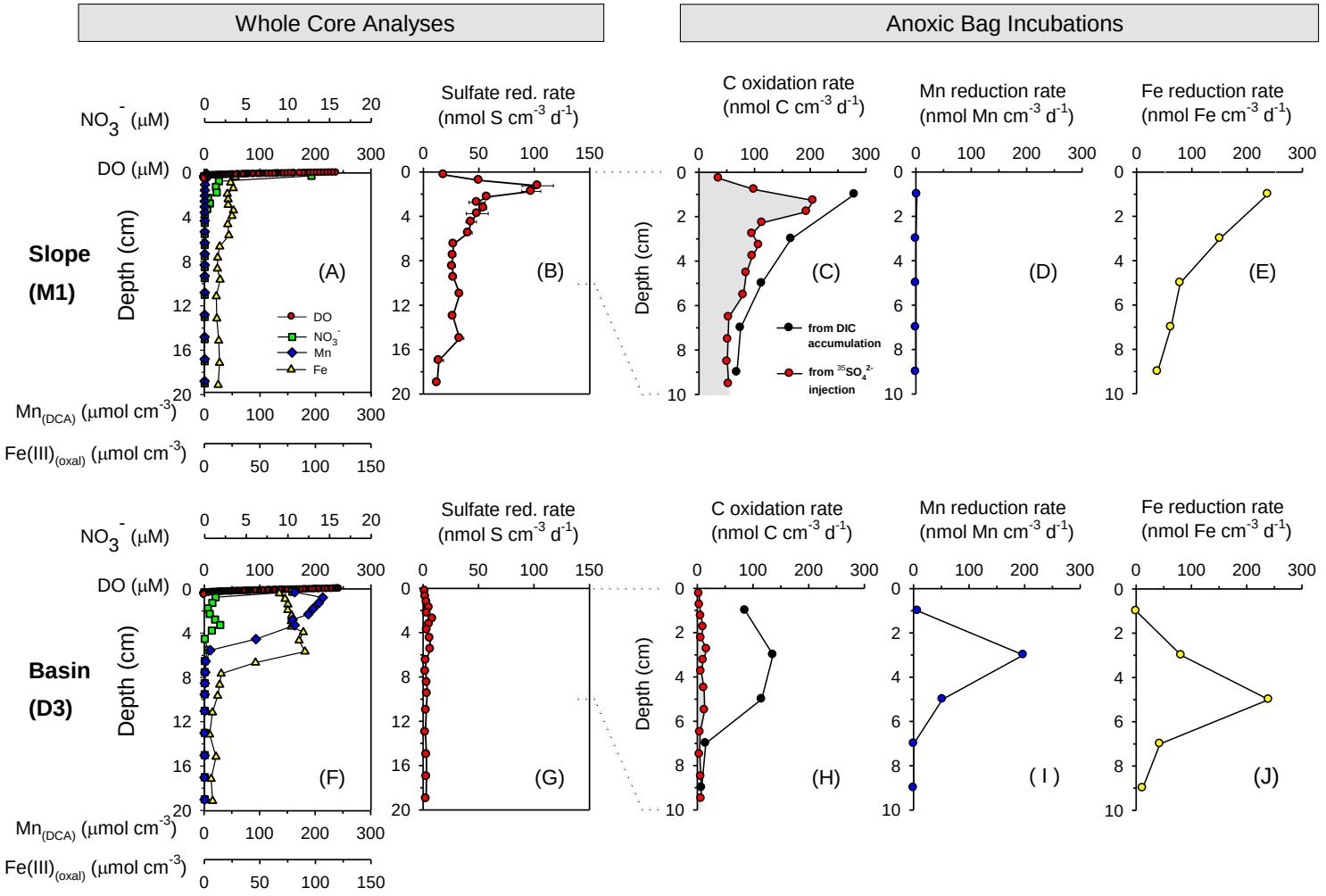

Hyun et al. – Figure 6

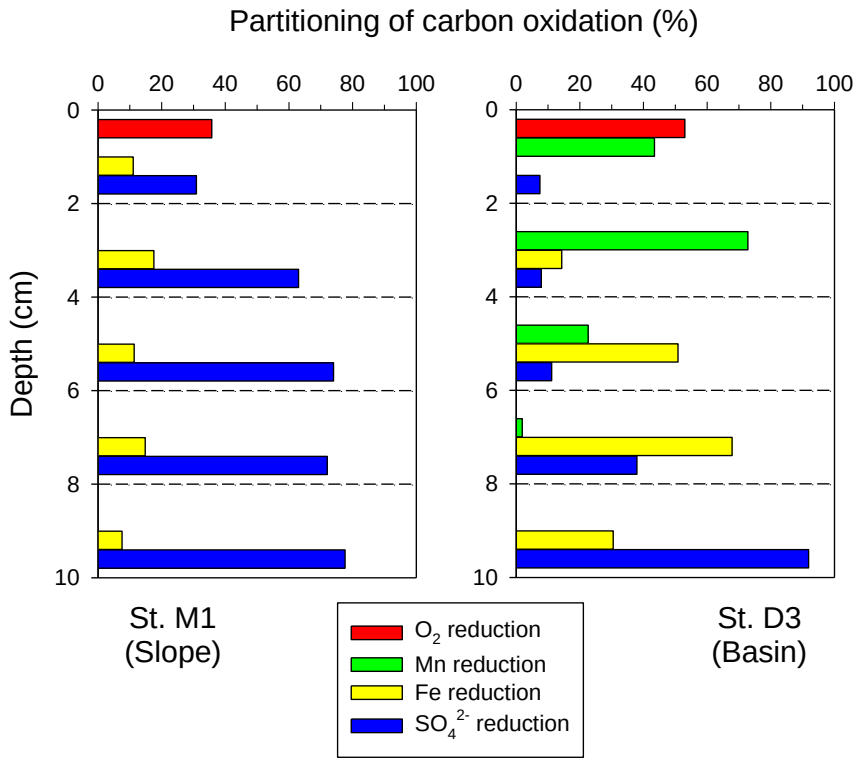

Hyun et al - Figure 7